9

Luminescence spectra of quantum dots in microcavities

F. P. LAUSSY, Walter Schottky Institut, Germany, E. DEL VALLE, TU München, Germany, A. LAUCHT, Walter Schottky Institut, Germany, A. GONZALEZ-TUDELA, Universidad Autónoma de Madrid, Spain, M. KANIBER and J. J. FINLEY, Walter Schottky Institut, Germany and C. TEJEDOR, Universidad Autónoma de Madrid, Spain

Abstract: The physics of strong light-matter coupling of a quantum dot in a microcavity is described at its most fundamental level, that of the Jaynes–Cummings Hamiltonian. Dissipation, dephasing and incoherent excitation are included in the Lindblad form to account for the most important experimental degrees of freedom. We focus on the photoluminescence emission and elucidate the complexity that can arise from the delicate interplay of pumping and decay. A unified picture is presented of several regimes of excitation describing spontaneous emission, quantum nonlinearities and lasing. The theoretical findings are fully supported by experimental observations when systems with sufficiently high figures of merit are within reach.

Key words: cavity QED, microcavities, strong coupling, photoluminescence, power spectra, lineshapes.

9.1 Introduction

The past few years have witnessed rapid progress in the understanding of the nature of light-matter interaction in photonic semiconductor nanostructures. Such systems offer an appealing implementation of cavity quantum electrodynamics (QED) in the solid state, an avenue of exploration openly declared by Weisbuch and co-workers (1992) when they reported the first demonstration of strong light-matter coupling in a semiconductor. This seminal achievement utilised a planar quantum well (QW) embedded in a 2D microcavity, for which it is generally agreed that the normal-mode coupling that it realizes is a classical effect (Khitrova *et al.*, 2006) as it is well described in terms of Maxwell's equations coupled to the excitonic susceptibility. The primary focus quickly became to reduce the dimensionality of the system and move from 2D towards 0D in order to exploit cavity QED physics in the purest form with the minimal phase-space. Andreani *et al.* (1999) showed that

strong coupling (SC) in 0D systems was within reach of the semiconductor quantum emitters, and this was soon reported by Reithmaier *et al*. (2004) and Yoshie *et al*. (2004) in two consecutive and highly cited letters to *Nature*.

Cavity QED is a fundamental and, thus, highly multidisciplinary field. It was pioneered by Raizen *et al*. (1989), Thompson *et al*. (1992) and others using atoms in macroscopic cavities (Haroche and Kleppner (1989) give a good overview of the early years) but has now spread to various systems such as superconducting circuits (Wallraff *et al*., 2004; Astafiev *et al*., 2007) or nanomechanical resonators (Aoki *et al*., 2006). At the heart of the physics governing this diverse array of systems is the Jaynes and Cummings (1963) Hamiltonian that describes the interaction at the quantum limit of one-emitter and a single-mode of light. It is a widely studied system, with authoritative reviews such as that of Shore and Knight (1993), and is often alluded to as being a cornerstone of quantum optics. One has many options to place it in the semiconductor context, the most natural being to consider the most straightforward experimental data, for example the observed splitting in photoluminescence (PL), and describe results by exactly diagonalizing the coupling Hamiltonian. We will show that this is not appropriate. Another approach is to include the most relevant semiconductor degrees of freedom, keeping the system as close as possible to the original Jaynes–Cummings Hamiltonian, including spins or a few excited states. Results in this direction have been obtained by Yamaguchi *et al*. (2009), Ritter *et al*. (2010) and del Valle *et al*. (2010). However, since the system is quantum, it becomes quickly intractable and one needs to turn to other methods. Examples include those from semiconductor quantum optics (Haug and Koch, 1990) that use quantum many body theory and methods such as cluster expansion (Kira and Koch, 2008) to accommodate a more complex description of the specific properties of the semiconductor system under study. Leading work in this context has been presented by Gies *et al*. (2007), Richter *et al*. (2009), Carmele *et al*. (2010) and Wiersig (2010), some aspects of which are featured in this volume.

When we addressed this problem theoretically, somehow to our surprise we realized that there was still much room for new physics, even at the most fundamental level of description very close to the original Jaynes and Cummings model. With a few elementary but, with hindsight, obvious and necessary assumptions, we could achieve the best level of agreement with experimental data reported to date (Laussy *et al*., 2008; Laucht *et al*., 2009a). Much of the present text will give an overview of this claim. The point where one can account accurately for the observed data – gaining some nontrivial understanding in the process – is a starting point to explore and predict new regimes of operation. This will constitute the second part of our text, where we will discuss some aspects of the nonlinear quantum regime and lasing. Throughout, we will focus on the luminescence emission, and more specifically on the spectral lineshapes. We will also limit to the case of a

single quantum dot (QD) (see Laussy *et al*. (2011) for a generalization to N emitters). For brevity we will leave aside technical details and derivations, mainly presented by Laussy *et al*. (2009) and del Valle *et al*. (2009). Much of this work has later been compiled and detailed by del Valle (2010).

From the experimental point of view, the seminal 2004 reports of strong coupling in 0D semiconductor systems – in a pillar and a photonic crystal, respectively – have been naturally reproduced and extended by others, shortly thereafter by Peter *et al*. (2005) in a microdisk, then by Hennessy *et al*. (2007) and Press *et al*. (2007) who demonstrated the single-quantum character of the interaction, etc., and ourselves, in the work presented by Laucht *et al*. (2009a, 2009b), the main results of which we will summarize here.

9.2 The Jaynes–Cummings model

The most fundamental quantum model of light-matter interaction is given by Jaynes and Cummings (1963) (JC), who describe the case of exactly one-emitter – a two-level system with annihilation operator σ – coupled with strength g to a single mode of the electromagnetic field – an harmonic oscillator with annihilation operator a. The JC Hamiltonian reads (in units where $\hbar = 1$):

$$H = \omega_a a^\dagger a + (\omega_a - \Delta)\sigma^\dagger \sigma + g\left(a^\dagger \sigma + a\sigma^\dagger\right). \qquad [9.1]$$

We have introduced $\Delta = \omega_a - \omega_\sigma$, the detuning between the bare cavity frequency ω_a and bare emitter frequency ω_σ and will, in the following, take ω_a as the reference point for all the energies ($\omega_a = 0$). A remarkable feature of Equation [9.1] is that, as it conserves the number of excitations, its quantum dynamics is closed in 2×2 Hilbert subspaces and can therefore be solved exactly. We will encounter $|k\pm\rangle$ the '*dressed states*', or '*polaritons*', that arise in this process: these are pairs of states (labelled by $\pm$) that group into 'manifolds of excitation' (labelled by k). These are also popularly called 'rungs' to reflect the ladder like nature of the resulting excitation spectrum. The kth manifold has k quanta of excitation, distributed over the light field that is unbounded in its number of photons, and the emitter that can only be empty or excited.

The most fundamental and by far the most studied light-matter coupling case involves only one quantum, the system oscillating between the single-photon $|1, 0\rangle$ and the excited emitter $|0, 1\rangle$. The dressed states at resonance are $|1\pm\rangle = \left(|1,0\rangle \pm |0,1\rangle\right)/\sqrt{2}$. As a result of this oscillation, the PL spectrum splits into a doublet – *the Rabi doublet* – as pointed out in this context by Sanchez-Mondragon *et al*. (1983). As there is only one quantum exchanged between the two fields, the phenomenon is known as *vacuum Rabi splitting*

(VRS). We shall be greatly concerned in the following with this case but also with the one when the emitter is dressed by photons rather than by the vacuum.

Three years after Sanchez-Mondragon *et al.* (1983), it was noted by Agarwal and Puri (1986) that in order to compute a self-consistent PL spectrum, one has to take into account leakage of the photons from the cavity. With hindsight, this seems obvious since how can one detect, otherwise, luminescence? This has the consequence of linking any single manifold with all the others below, in a cascade of emission, with the vacuum as the final (long-time) solution.

Three years later, Carmichael *et al.* (1989) completed the picture by including also a finite lifetime for the emitter. Theoretically, a simple and powerful way to include dissipation is to shift to a density matrix ρ rather than a wavefunction $|\psi\rangle$. The equation of motion that supplements the Schrödinger equation is then the Liouville–von Neuman equation:

$$\partial_t \rho = -i\big[H,\rho\big] + L\rho, \qquad [9.2]$$

where the Liouvillian L describes the non-unitary, dissipative dynamics. For the case of lifetime, with decay rate γ_c ($c = a, \sigma$ for the cavity and dot, respectively), the Liouvillian reads:

$$L\rho = \sum_{c=a,\sigma} \frac{\gamma_c}{2}\left(2c\rho c^\dagger - c^\dagger c\rho - \rho c^\dagger c\right), \qquad [9.3]$$

using c both as an index for parameters and operators. The eigenenergies can still be obtained exactly in the presence of this form of dissipation. Their derivation is given by del Valle *et al.* (2009). They read:

$$E_\pm^k = k\omega_a - \frac{\Delta}{2} - i\frac{(2k-1)\gamma_a + \gamma_\sigma}{4} \pm \sqrt{\left(\sqrt{k}g\right)^2 - \left(\frac{\gamma_a - \gamma_\sigma}{4} + i\frac{\Delta}{2}\right)^2}. \qquad [9.4]$$

The eigenenergies [9.4] are complex as a result of the dissipative part. They are shown in Fig. 9.1a for the first three manifolds (and vacuum $|\text{vac}\rangle$), where we have broadened the resonance at $\Re(E_\pm^k)$ with their imaginary part to reflect the linewidths of the transitions. This structure is known as the '*Jaynes–Cummings ladder*'. The energies of the states on the JC ladder cannot be observed directly, but arise when the system undergoes a transition from one state to the other. Such a transition naturally occurs when one excitation decays. The type of decay described by Equation [9.3] brings

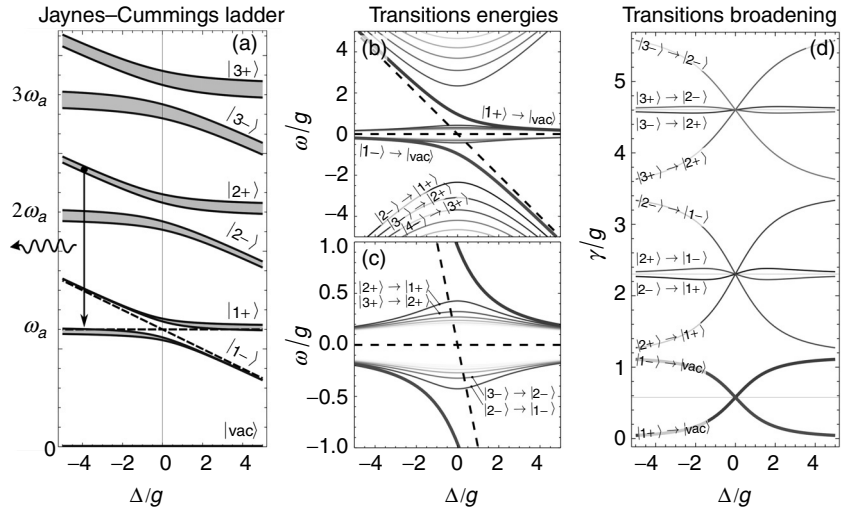

9.1 (a) The Jaynes–Cummings ladder, up to the first three rungs. Bare states are shown in dashed lines in the first manifold. Their crossing point marks the resonance. Transitions between neighbouring rungs account for the observed peaks in the spectra, as sketched by the emission of a photon from the initial state $|2+\rangle$ to the final one $|1-\rangle$. The set of frequencies that arise in all possible such processes is shown in (b), (c) with, in thick lines, the upper and lower polaritons of the first manifold, which can be seen in isolation by exciting the system weakly. Inner transitions are stronger in the cavity emission, but they are closely spaced. All nonlinear transitions have a large broadening, increasing with the manifold number, as shown in (d). Parameters are those estimated for the experiment discussed in the text: $\gamma_a/g \approx 1.15$ and $\gamma_\sigma/g \approx 0.00334$.

it (to first order) to the neighbouring manifold below. A possible transition is sketched in Fig. 9.1a bringing the system from $|2+\rangle$ to $|1-\rangle$. There are two main channels of emission for this transition: by the cavity mode or by the QD into a continuum of background modes (also known as leaky modes). They differ in one important aspect: the cavity suppresses transitions involving a change of the polariton branch ($\pm \to \mp$) and strengthens same-branch transitions ($\pm \to \pm$) with emitted intensities proportional to:

$$\left|\left\langle k-1,\pm\middle|a\middle|k,\pm\right\rangle\right|^2 = \frac{\left|\sqrt{k}+\sqrt{k-1}\right|^2}{4}, \qquad [9.5]$$

$$\left|\left\langle k-1,\pm\middle|a\middle|k,\mp\right\rangle\right|^2 = \frac{\left|\sqrt{k}-\sqrt{k-1}\right|^2}{4}, \qquad [9.6]$$

whereas the QD emission is equal in any of the four possible combinations:

$$\left|\left\langle k-1,\pm\left|\sigma\right|k,\pm\right\rangle\right|^2=\left|\left\langle k-1,\pm\left|\sigma\right|k,\mp\right\rangle\right|^2=\frac{1}{4}. \qquad [9.7]$$

This is because in a transition of the type of Equation [9.5], the final and initial states are, up to a photon, identical. The emitted photon can be any of the k available ones, and the transition is, therefore, k-fold enhanced. This is a manifestation of Bose statistics that follows from the indistinguishability of which photon is eventually emitted. In the limit of high number of excitations, the photon field factors out and becomes classical. On the other hand, regardless of the state of the system (and the number of excitations), the emission by the dot involves a complete alteration of the quantum state, since annihilation of the QD excitation collapses it onto a bare state. As a result, whereas photons emitted by the cavity and QD both carry away the same energy difference between initial and final states, the QD photon is a better probe of the system dynamics, which it perturbs intrinsically. The energy difference involved in both cases reads:

$$E_{\beta_k}^{k}-\left(E_{\beta_{k-1}}^{k-1}\right)^{*}, \qquad [9.8]$$

with β_k and $\beta_{k-1} = \pm$, yielding four resonances for each manifold, which we will term *outer transitions* for $(\beta_k, \beta_{k-1}) = (+, -)$ or $(-, +)$ and *inner transitions* for $(+, +)$ and $(-, -)$. These transitions are shown in Fig. 9.1b and, zoomed on the inner transitions, in Fig. 9.1c. A favoured way of probing these transitions is the PL that this gives rise to. Through an argument known as the input–output formalism, the PL spectrum corresponds to the mean number of excitations at frequency ω, that is, in second quantization formalism, as an average over the number operator for this mode, $S_c(\omega) \propto \langle c^{\dagger}(\omega)c(\omega)\rangle$ where again $c = a$ for the cavity PL spectrum, or $c = \sigma$ for the QD direct emission. By Fourier transform from frequency ω to real time t, we obtain the PL with the Wiener–Khintchin theorem: $S_c(\omega) \propto \Re\int_0^{\infty} G^{(1)}(t,\tau)\exp(i\omega\tau)\mathrm{d}t\mathrm{d}\tau$. Computing from Equation [9.2] the quantity of interest, the two-time photon autocorrelator

$$G^{(1)}(t,\tau)=\left\langle c^{\dagger}(t)c(t+\tau)\right\rangle \qquad [9.9]$$

is readily achieved using the so-called quantum regression theorem (QRT), which is a standard quantum-optics technique that we will not develop here. However, we emphasize that in the course of applying the QRT, a physically

transparent decomposition of $S_c(\omega)$ – presented and amply detailed by Laussy *et al.* (2009) and del Valle *et al.* (2009) – can be performed semi-analytically in terms of Lorentzians and dispersive parts:

$$S_c(\omega) = \frac{1}{\pi}\sum_p \left(L_p^c \frac{\gamma_p/2}{\left(\omega-\omega_p\right)^2 + \left(\gamma_p/2\right)^2} - K_p^c \frac{\omega-\omega_p}{\left(\omega-\omega_p\right)^2 + \left(\gamma_p/2\right)^2} \right) \quad [9.10]$$

where ω_p are the possible transitions in the system, that is, the real part of Equation [9.8] and γ_p their corresponding broadening (full width at half maximum, FWHM), that is, twice the imaginary part of Equation [9.8]. The Lorentzian corresponds to the decay of a dressed state, this lineshape being the one that arises from the decay of a particle with a finite lifetime. The dispersive part is an interference term that arises when the dressed states overlap in energy, and affect each other. This is the case for instance when the system is not in very strong coupling or when pumping pushes dressed states against each other, as we shall discuss later. The problem of PL spectra is, therefore, reduced to computing the coefficients K_p and L_p that depend on such factors as the dynamics, the initial state, the channel of detection, etc. We will now show that, although the essential physics is indeed embedded in the JC ladder, one should not limit one's understanding to this picture only, but should consider the possible impact of the weighting coefficients, which can disguise the final result in a form far from that one has in mind from the sole Fig. 9.1.

The thick lines in Fig. 9.1 are the VRS that arise from transitions from the first manifold to the vacuum, a situation realized at very small pumping when only the first rung is excited. The amount of signal is proportional to the amount of time the first manifold is excited and available to emit. As long as only this fraction of occupancy is enhanced without populating higher manifolds, the system is in a linear regime. This is the first regime to achieve in the investigation of quantum light-matter coupling and the one which has, therefore, attracted the most experimental attention. At the time of writing, this starting point is still a challenge for most experimental groups and only a handful of laboratories are able to produce it on a regular basis. We shall discuss it thoroughly in the following sections, survey the main experimental findings obtained by our group, which are representative of the situation at large, and in the latter sections come back to the higher rungs of the ladder, or higher manifolds of excitation. This is a topic of considerable current research activity and one for which little if any compelling experimental results are currently available.

9.3 Luminescence spectra

9.3.1 Luminescence spectra of spontaneous emission

To describe the linear regime, it is instructive to start with the simplest possible consideration, which is that of spontaneous emission of an initial state. In the atomic-cavity framework, one has in mind the excited state of the atom as an initial state. When Andreani *et al.* (1999) initiated the quest for this regime in the solid state, they also considered the spontaneous emission of the QD. In the semiconductor case, in contrast to the atomic-cavity configuration, the cavity emission spectrum is more conveniently detected, rather than the radiation field of the emitter. The calculation for cavity emission was performed by Cui and Raymer (2006) and extended by Naesby *et al.* (2008) to the case of nonzero detuning.

Furthermore, semiconductors are complicated solid state systems where even in an epitaxially perfect structure, the QD is coupled to many baths and other degrees of freedom (carriers in higher states, phonons, etc.) To describe incoherent excitation through the wetting layer, one cannot always assume the preparation of a pure initial state for the QD alone. For instance, injecting electron-hole pairs to bring the QD of interest in its excited state could also excite many other QDs, not in SC, which capture these excitations and convert them into photons. As a result, the strongly coupled dot effectively starts the dynamics with a photon as the initial state. Tarel *et al.* in this volume show that even in samples where only one QD is present, there are other routes for the system to populate the cavity. As a consequence, in a semiconductor, the *spontaneous emission of a photon* is a natural scenario. This has great bearing on the problem because the PL spectrum can differ greatly from one initial state to the other. This is shown in Fig. 9.2 where the cavity PL spectrum is displayed for the excited QD (solid), a photon (dashed) or an upper polariton (dotted) as an initial state. Note that the Rabi splitting can be more readily resolved (larger splitting and larger contrast) when the initial state of the system is a photon rather than an exciton. The reason why is clear physically: the cavity PL spectrum is a Fourier transform of Equation [9.9]. When not in very strong coupling, starting as a photon triggers the $G^{(1)}(t, \tau)$ dynamics from the beginning, whereas starting as an exciton, the two-time photon autocorrelator remains initially zero (the photon field being zero) and has to wait a Rabi cycle to be fully initialised. In the intervening time, decay has damped intensity of both fields and the $G^{(1)}$ dynamics is weakened by as much, explaining why the Rabi splitting is spoiled. In the case of the polariton, the difference is even qualitative since the spectrum reduces (almost perfectly) to a singlet, namely, the polariton line (one would indeed not expect a lower polariton to show up when decaying an upper polariton). The dynamics of $G^{(1)}(t, \tau)$is shown in Fig. 9.2 at

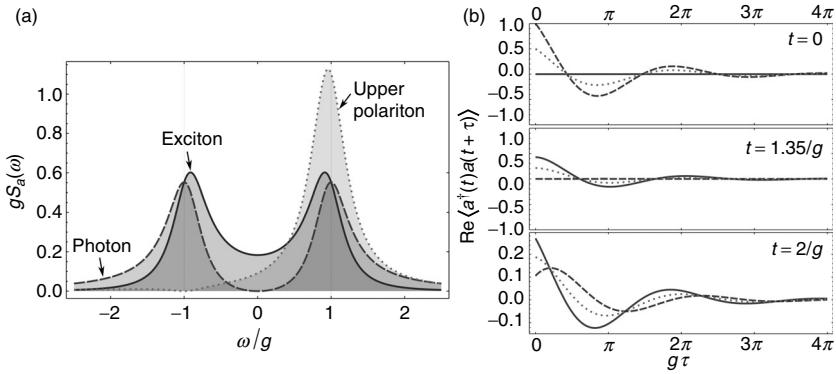

9.2 (a) PL spectra of spontaneous emission for three different initial states: an exciton $|0, 1\rangle$ (solid line), a photon $|1, 0\rangle$ (dashed) and an upper polariton $|1+\rangle$ (dotted). The initial state influences significantly, sometimes qualitatively, the observed spectrum. (b) Corresponding Rabi oscillations of $G^{(1)}(t, \tau)$ at three different times, accounting for these differences. Starting as a photon gives more time for the system to undergo coherent dynamics and thus leads to a better resolved Rabi splitting. Note that the last row has a different scale for the y-axis. Parameters are the same as before: $\gamma_a/g \approx 1.15$ and $\gamma_\sigma/g \approx 0.00334$.

three different times for these three different initial conditions, illustrating the above discussion. Note that the dynamics when starting as a polariton is mostly decaying in t whereas photons and excitons undergo non-stationary oscillations. This simple point is of considerable importance because there is a popular practice of reading off the splitting between the dressed states from the splitting in PL, that is, in Equation [9.10], to ignore the effect of the dynamics. We shall see in the following that the error induced by doing so can be arbitrarily large.

To conclude this section, let us remark that we have discussed how the channel of detection – direct QD or cavity emission – influences the observed PL through arguments of strength of transition from higher excited states in the ladder such as those contained in Equations [9.5]–[9.7]. By symmetry, one can see that the initial quantum state also plays a similar role in the QD emission. In the linear regime, the following correspondence is satisfied by interchanging a and σ everywhere in the equations and their solutions: the cavity PL spectrum of an exciton (respectively, photon) as the initial state is the same as the QD PL spectrum of a photon (respectively, exciton) as the initial state. Therefore, when exciting the emitter, it is more advantageous to observe its spontaneous emission, as is indeed the case with atomic-cavity QED, for instance. This is one reason why QDs in microcavities struggle to exhibit SC, a tendency that becomes more acute for more 'atom-like' systems. We will show below that strong coupling experiments with semiconductor

QDs have been aided by a so-called *cavity feeding* mechanism that favours the initial state of the system to be photon-like. For systems in very strong coupling, such as in circuit QED, the Rabi dynamics is sustained over such a large number of cycles so that its initial state, or channel of detection, does not matter. In this case one can focus on the pure quantum dynamics of Equation [9.1] with little importance given to dissipation. This is a luxury not yet affordable in semiconductors.

9.3.2 Luminescence spectra under incoherent pumping

From a practical point of view, the fact just discussed – that the initial quantum state affects the observed PL spectrum – could be used experimentally to favour observation of the splitting. There has not been, so far, any such attempt in this direction, neither to control nor to merely alter the quantum state of the system, making it more photon-like or exciton-like on purpose. Naturally, exciton, photon or polariton are particular cases, and a realistic situation would call for an arbitrary mixture of exciton and photon. Here again, the density matrix formalism becomes handy, since instead of considering a pure initial state, one can now contemplate statistical mixtures. However, rather than computing the PL spectrum of a given state ρ at $t = 0$ it is more rewarding to add self-consistently the excitation process in the description of the system. This has been done for instance by Perea *et al*. (2004) for excitonic pumping. As we have said that both the expected QD excitation scheme and its derived cavity feeding are conceivable in semiconductors, we take the more general approach of including two pumping schemes, cavity pumping at rate P_a and exciton pumping at rate P_σ. We shall be concerned in this text with incoherent pumping only, in which case the equation of motion for the density matrix is supplemented with, following del Valle *et al*. (2009):

$$L\rho = \sum_{c=a,\sigma} \frac{P_c}{2}\left(2c^\dagger \rho c - cc^\dagger \rho - \rho cc^\dagger\right). \qquad [9.11]$$

At the outset, there is no reason to constrain P_c in any particular way, and we shall assume for generality that they are independent, though they can assume a more particular form from a given underlying microscopic mechanism. For instance, the particular case discussed above of cavity feeding by weakly coupled spectator QDs is treated by Averkiev *et al*. (2009) and del Valle and Laussy (2010a). Yao *et al*. (2010) criticized divergences that arise, for instance when $P_a > \gamma_a$, and concluded that the master equation must be unphysical. They considered the particular case of our model where $\gamma_a = \kappa(\bar{n} + 1)$ and $P_a = \kappa\bar{n}$ are linked through thermal equilibrium relationships

as the only possible alternative. Such divergences are, however, intrinsic in this system, they mark the onset of lasing, and are present even with no explicit cavity pumping in the limit of vanishing γ_a, in which case the coherence built by the QD is enough to grow the cavity field without bounds. This shows that divergences certainly do not invalidate the more general unconstrained model, which always has a proper finite-time solution (only its steady state is not always assured, which is, however, perfectly acceptable for a dynamical system).

Although we are concerned with spectral lineshapes in this text, we have to consider the closely related observables that are the average cavity population $n_a = \langle a^\dagger a \rangle$, the average QD occupation $n_\sigma = \langle \sigma^\dagger \sigma \rangle$ and the second-order correlator at zero delay $g^{(2)}(0) = \langle a^\dagger a^\dagger a a \rangle / n_a^2$. Other quantities such as statistics of the photon numbers or purity of the state, $\mathrm{Tr}(\rho^2)$, are given by Laussy and del Valle (2010). Those of interest here are shown in Fig. 9.3 for various values of γ_a as a function of QD pumping only (with $P_a = 0$). We choose n_a, Fig. 9.3a, to illustrate the various regimes that the system is going

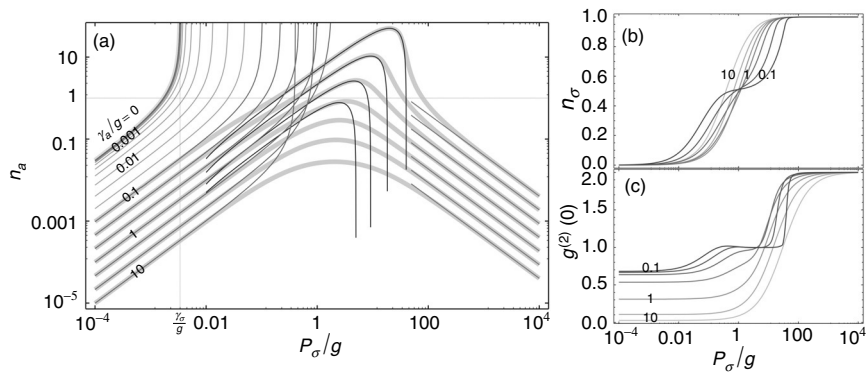

9.3 Single-time observables: (a) cavity population n_a, (b) QD population n_σ and (c) two-photon counting correlator $g^{(2)}$, for γ_a/g varying exponentially between 10 and 0.1, as a function of QD pumping. In (a) the exact population is plotted in thick lines and spans the whole pumping range. Superimposed are analytical approximations in the various regimes of operations. On the left is shown the linear model (with two Bose fields), which is a good approximation of the JC in the linear regime. It is extended to values of γ_a, which tend exponentially to zero. These solutions become exact over their entire range of validity when $\gamma_a \to 0$, with a divergence at $P_\sigma = \gamma_\sigma$, the threshold for lasing. In the middle part of (a) is shown the lasing-regime approximation, which is quantitatively good for the four upper cases only. In the right part of (a) is shown the thermal approximation. Observables in (b) and (c) behave as expected for these regimes: inversion (respectively, saturation) of the dot with uncorrelated (respectively, bunched) statistics for the photon counts in the lasing (respectively, thermal) regime.

through. The thick lines that span the whole pumping range are the exact populations, computed numerically. The thin lines, which take roughly one third each of the pumping range, are analytical approximations. When they agree with the numerical result, they define the various regimes of operation. The approximate expressions for these three regimes are given by:

$$n_a \approx \frac{4g^2}{(\gamma_a+\gamma_\sigma)\left(4g^2+\gamma_a\gamma_\sigma\right)} P_\sigma \quad \text{linear regime (left)}, \tag{9.12}$$

$$n_a \approx \frac{\gamma_\sigma+P_\sigma}{2\gamma_a}\left(1-\frac{2\gamma_\sigma}{\gamma_\sigma+P_\sigma}-\frac{\gamma_\sigma+P_\sigma-\gamma_a}{4g^2/\gamma_a}\right) \quad \text{lasing regime (middle)}, \tag{9.13}$$

$$n_a \approx \frac{4g^2}{\gamma_a} P_\sigma^{-1} \quad \text{quenched regime (right)}. \tag{9.14}$$

These results follow from Laussy *et al*. (2009), del Valle *et al*. (2009) and del Valle and Laussy (2010a) (similar results can be obtained for n_σ, $g^{(2)}(0)$, etc.) We will now address these various regimes in turns.

9.3.3 Luminescence spectra in the linear regime

At small pumping (around $P_\sigma/g < 0.01$ for the parameters of our experiment), when only the first manifold is significantly occupied, the two-level system σ (a Fermi operator that anticommutes) can be replaced in good approximation by a harmonic oscillator operator b (a Bose operator that commutes), like a for the cavity photon. This has the considerable advantage that all observables, including PL spectra, can be solved exactly under incoherent pumping. Disposing of closed-form expressions allowed us to provide the first quantitative descriptions of experimental data, as reported by Laussy *et al*. (2008). Equivalently, in this regime one can solve the Jaynes–Cummings system truncating in the first manifold, as was done by Laucht *et al*. (2009a), with the added advantage of extending the domain of applicability beyond the linear regime. This can be done providing that the coupling is sufficiently weak such as to ensure that the excitation number in the system never exceeds unity. In the weak coupling (WC) regime, the validity extends to the whole pumping range. An example adapted from Laucht *et al*. (2009a) will be discussed below. Good agreements between such types of model and the experiment have also been obtained by other groups, for instance by Münch *et al*. (2009).

The two-coupled oscillators, or *linear model*, is valuable in its own right, not only when $n_a \ll 1$. For arbitrary populations, it describes for instance the ground state of QW exciton-polaritons (see Kavokin *et al*.'s (2011)

textbook). Imamoglu and Ram (1996), Rubo *et al.* (2003), Laussy *et al.* (2004) and others used it to describe the dynamics of their Bose–Einstein condensation. The PL spectrum of such models has been computed by Porras and Tejedor (2003) (paying special attention to interactions). More related to our present topic, this also describes the case of large QDs in microcavities, where the emitter can accommodate more than one excitation, a situation studied by Laussy *et al.* (2006). We shall now describe the linear model in its most general form, but if the intent is to apply it to the small pumping case of the JC system, one should be careful to make sure there is no deviation from the full JC system, for example by checking numerically the population with formula [9.12]. (This precaution should also be taken with the truncated JC model.) When all these models converge, results are exact so far as first order observables – such as populations and PL spectra – are concerned. Second and higher order correlations, on the other hand, are not properly described. The counting statistics, $g^{(2)}(0)$, for instance, is always equal to 2 in the linear model (and zero in the truncated JC), whereas it can take intermediate values for the JC system, as shown in Fig. 9.3c, being the closer to zero (antibunching), the larger the decay rate (showing that systems far from SC may have some value for generating quantum light).

By including pumping in the linear model, one changes the conventional criterion for SC, which, defined by the condition of emergence of dressed states, reads:

$$\left|\gamma_a - \gamma_b\right| < 4g. \qquad [9.15]$$

Including pumping, it modifies to:

$$\left|\left(\gamma_a - P_a\right) - \left(\gamma_b - P_b\right)\right| < 4g. \qquad [9.16]$$

That is, the meaningful decay rates – which, in the spontaneous emission case of Equation [9.15], are the decay rates for one excitation (γ_a and γ_b) – become the decay rates of the modes. Since they are bosonic here, they may acquire under continuous excitation a longer effective lifetime: the system still loses individual excitations at the rate γ_c ($c = a, b$) but the states that undergo the coupling dynamics are not single quanta anymore but a 'condensate' of excitations that are sustained in the system by the interplay of pumping and decay. In the left part of Fig. 9.3a, we plotted the population following from the linear model (with Bose stimulation), which features the divergence associated with the formation of the condensate. When $P_c \to \gamma_c$ (from below) the mode becomes infinitely lived with an infinite coherence time and its linewidth vanishes accordingly. Therefore, pumping may help SC.

On the other hand, being of an incoherent nature, it also disrupts coherence by randomizing the phase and can also, if it is too large, tend to bring the system into the WC regime. Therefore, incoherent pumping represents a trade-off between favouring and spoiling coherence. With the coupling strength g providing the unit, there are four parameters that determine the phases of weak and strong coupling in this wider picture that includes pumping: γ_c and P_c. The four-dimensional phase-space that results is represented with two 3D cuts in Fig. 9.4 (cutting in the plane $\gamma_b = 3g/59$, this being the parameter of our experiment presented below) and in Fig. 9.5 (cutting in

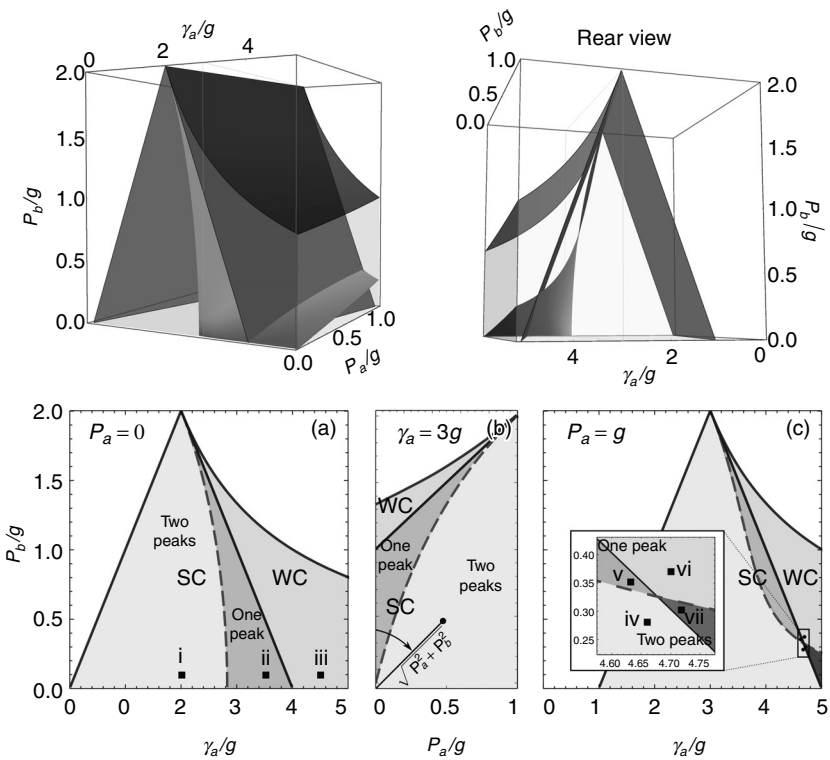

9.4 Phase space of coupling between two Bose fields. Upper row, phases in the (γ_a, P_a, P_b) space (front and rear view). Lower row: cuts in the above views, in the (γ_a, P_b) ((a) and (c)) and (P_a, P_b) (b) subspaces. The fourth parameter γ_b/g is the one of the experiment ≈ 3/59. In addition to the regions of SC and WC, the darker shaded area shows regions where the PL spectrum is single peaked in SC or double peaked in WC, which is unexpected from the dressed states picture. One can observe the splitting either by making the coupling stronger (decreasing γ_a/g) as shown in (a) and/or providing a photon content to the system, as seen in (b)–(c). The points (i)–(iii) mark the position of the spectra plotted in Fig. 9.6 and (iv)–(vii) in Fig. 9.7.

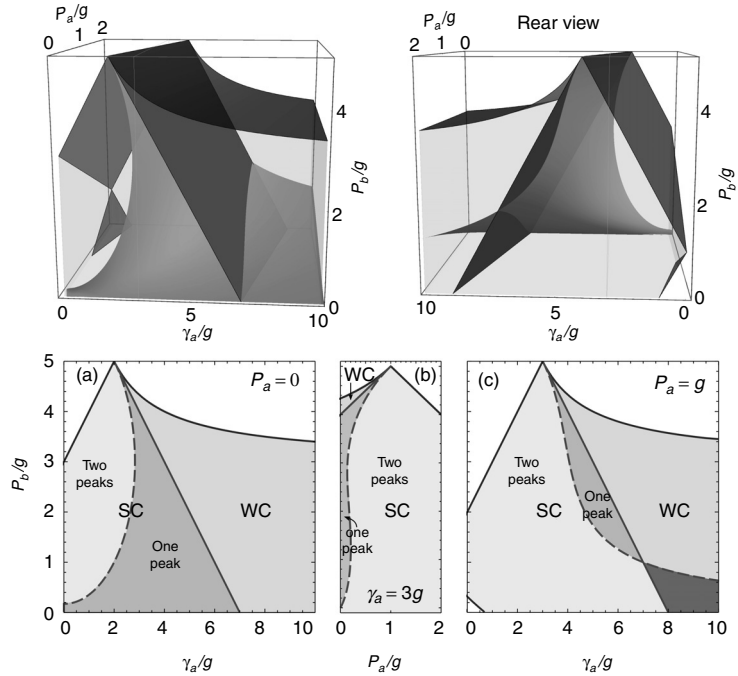

9.5 Same as Fig. 9.4 but for $\gamma_b = 3g$. In this case, the area of splitting visibility is very much reduced and no splitting is observed at any value of γ_a without nonvanishing cavity feeding. Even the spontaneous emission of a photon does not result in a doublet and dynamics of the pump is required to resolve the splitting.

the plane $\gamma_b = 3g$). The region admitting a steady state is bounded, since the loss of particles that increases with the number of excitations is balanced by Bose stimulation of pumping, and one should, thus, exclude cases where more particles are injected at any given moment than are lost, otherwise the system increases without bounds. The boundary can be found by solving the equation $n_a \to \infty$ for Equation [9.12]. We come back to the physical meaning of this behaviour, which is an instability driving the system to lasing, when discussing the JC system.

The conditions of convergence are given by $\gamma_a + \gamma_b > P_a + P_b$ and $4g^2 > -(\gamma_a - P_a)(\gamma_b - P_b)$. The first condition determines the boundary on the SC side and shows that it is a hyperplane. The second determines it on the WC side and shows that it has a curvature, given by the effective Purcell parameter $4g^2/[(\gamma_a - P_a)(\gamma_b - P_b)]$. Within the area of convergence, another hyperplane separates the SC and WC spaces. The structure is, therefore, simple enough albeit in a 4D space. In any 2D cut, the SC space is enclosed in a polygon (on the 2D cuts shown in Figs. 9.4 and 9.5, the SC is enclosed within a

triangle, where in Fig. 9.5c, the lower-left corner is cut off). SC here corresponds to the existence of dressed states at resonance, that is, existence of nonzero ω_p.

A less fundamental quantity, but one that attracts a greater experimental interest, is the observed splitting in the PL spectrum. This has a much more intricate behaviour, which, for one thing, extends into both SC and WC spaces. The boundary between regions where the cavity PL spectrum is single-peaked and double-peaked is shown in the 3D plots as the surface enclosed in the region of convergence and in dashed lines in the 2D cuts of these. The analytical expression for this can be found in Gonzalez-Tudela *et al*. (2010b; there is a typo in Equation [9.3] in this text, Γ_b should be replaced everywhere by $-\Gamma_b$). Figure 9.4a is the case of no cavity pumping (the front face of the 3D representation). There, the one-peak area fully encloses the WC region and overlaps the SC region on its high-γ_a flank, showing that, because the splitting-to-broadening ratio of the polaritons becomes too small when SC becomes weaker, the ability to resolve the Rabi doublet is lost.

PL spectra for the points marked i, ii, iii are shown in Fig. 9.6, where one sees this fact spelled out by the decomposition from Equation [9.10] into dressed states and dispersive parts. If we progress along the P_a axis in Fig. 9.4, we see that this boundary is quickly shifted away from most of the SC region. For the reasons explained in the SE emission case, providing a photon character to the effective quantum state (by the interplay of pumps and decays) makes the doublet in PL more apparent, with a larger splitting and better contrast. Interestingly, by crossing into the WC region, this brings us into another region that goes against naive expectations since, although in WC, the system now presents two peaks at resonance. This latter case also has a clear physical origin. It arises when looking at the emission of a broad mode (say the cavity) coupling weakly to a narrower one (the QD) with the system starting in the state of the broad mode. The latter undergoes its

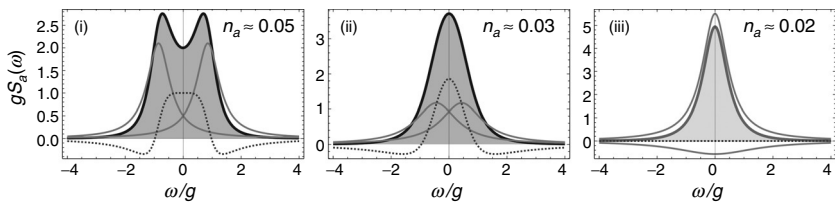

9.6 PL spectra (thick filled) for the points marked (i)–(iii) in Fig. 9.4. Dressed states are shown in thin lines and the interference term in dotted lines. The first two cases are in SC with splitting of the dressed states. The splitting to broadening ratio and crucially the interference term make the observed PL spectrum split in (i) but not in (ii). Third case is in weak coupling with degenerate dressed states, one being negative, and no interference term.

decay in the vacuum except for the frequency where it is coupled, albeit weakly, to the other mode, which serves as the favoured recipient for the de-excitation. As such, the effect evokes a Fano resonance, although the lineshape does not fit and, interestingly, has the lineshape of an electromagnetically induced transparency (EIT) interference (namely one Lorentzian carving a hole into another one). EIT is known to have a deep connection with the Autler–Townes splitting, which arises from a dressed state splitting and, thus, corresponds in our case to the Rabi splitting. We find here, at a more fundamental level, that such distinct phenomena share the same intimate connections in the simplest possible model of two-coupled harmonic modes. The final PL shapes change smoothly when crossing from the WC to the SC transition, although the underlying dynamics undergoes a dramatic change (going from real to complex valued correlators).

We have shown in Fig. 9.4 the case $\gamma_b \approx 0$, which corresponds to our experimental system. Here we see that observing a splitting in PL demands, in the absence of cavity feeding, a better figure of merit than that required for SC. Progressing in the 4D phase space, now in the direction of increasing γ_b, we will see that in the absence of cavity feeding, the area where a single peak at resonance is observed in PL extends dramatically in the SC region. In the case shown in Fig. 9.5 of $\gamma_b = 3g$, at vanishing pumping, splitting is never observed! One must either increase the QD pumping to enhance SC by increasing the effective lifetime of the mode, or bring in a nonzero photon pumping to change the photon state of the system. Although we have shown the case of wider generality where n_a and n_b can take any value, this discussion remains relevant for the limiting case of vanishing excitation of the JC system. Panels (b) in Figs 9.4 and 9.5 show in the P_b, P_a subspace how one or two peaks are resolved by tilting the angle determined by the ratio of P_b/P_a. Even for non-vanishing values, this angle is more crucial than the magnitudes of pumping themselves and the renormalization that they lead to. These four possibilities are explored by going around the intersection shown in Fig. 9.4c (zoomed in inset) with spectra iv–vii shown, together with their decomposition into dressed states and interferences, in Fig. 9.7. All these results combined show that a splitting in PL is neither a sufficient nor necessary condition of SC.

9.4 Experimental implementations and observations

The experimental implementation is naturally much more complex than the ideal two-level system coupled to a cavity that has just been presented. The QD, which we have used as a synonym for 'two-level system' in the theoretical model, exhibits other features in a real system and more particularly so in the semiconductor case. Regardless of the experimental system, the strong-coupling physics calls for high quality, low mode-volume cavities.

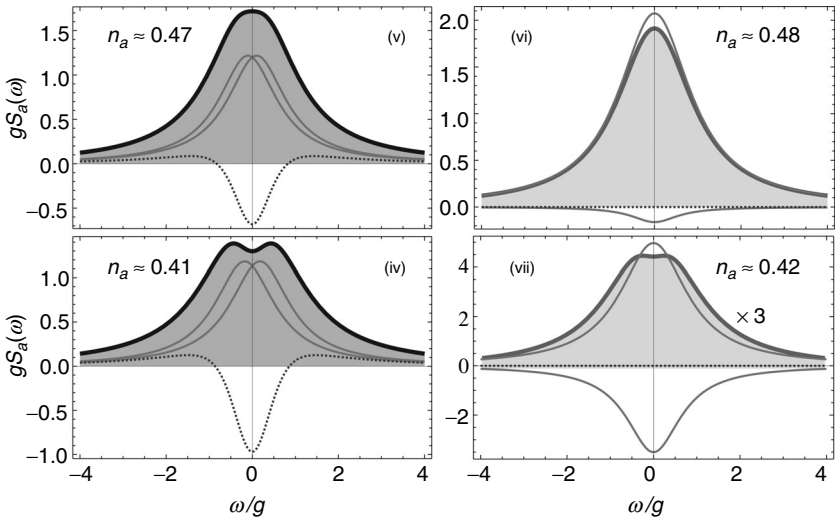

9.7 Same as Fig. 9.6 for the points marked (iv)–(vii) in Fig. 9.4, showing all configurations where (iv) a doublet is seen in SC (as expected), (v) a singlet is seen in SC (unexpectedly), (vi) a singlet is seen in WC (as expected) and (vii) a doublet is seen in WC (unexpectedly). Here again the criterion to define SC is the splitting of dressed states. The observed cavity spectrum changes smoothly over these four regions and is thus not a reliable indicator of SC in not-very strong coupling. As (vii) is dwarfed by the decomposition, the PL spectrum has been magnified by a factor of 3.

Two-dimensional photonic crystal defect microcavities containing low-density semiconductor QDs have proven to be a successful approach for realizing such structures in the solid state. An artistic view of such a device is presented in Fig. 9.8a. The basic structure of the underlying QD samples studied is shown in the inset and is based on GaAs *p–i–n* photodiode structures grown by molecular beam epitaxy. The nominal layer sequence is as follows: firstly, we deposit a 500 nm thick, *n*-type ($n = 2 \times 10^{18}$ cm^{-3}, Si-dopant) $Al_{0.8}Ga_{0.2}As$ sacrificial layer followed by a 35 nm thick, *n*-type GaAs lower contact layer ($n = 2 \times 10^{18}$ cm^{-3}, Si-dopant). This is followed by a 110 nm thick intrinsic GaAs waveguide core into the centre of which we grew a single layer of QDs by depositing 7.36 ML of $In_{0.4}Ga_{0.6}As$ at 595°C and a rate of 0.04 MLs^{-1}. A 35 nm thick *p*-type ($p = 2 \times 10^{19}$ cm^{-3}, C-dopant) GaAs top contact was then grown to complete the structure. A single layer of InGaAs self-assembled QDs with an areal density < 20 μm^{-2} are incorporated in the centre of the intrinsic region of the device. Subsequently we established a 5 × 5 square array of photonic crystals with defect nanocavities, which were placed using a combination of electron beam lithography and Cl_2-Ar reactive ion etching as shown in Fig. 9.8b. The photonic crystal consists of

a lattice of cylindrical air holes (radius r) arranged in a hexagonal lattice with period $a = 260$ nm and $r/a = 0.3$. Nanocavities were formed by omitting three missing holes at the centre of the photonic crystal. The L3 nanocavities support six strongly localized modes within the two-dimensional photonic bandgap with quality-factors ranging from $Q = 3000$ to 15 000. This allows us to perform measurements both in the weak and strong-coupling regime of the light-matter interaction.

To increase the quality factor of the established cavities, we detuned the outer holes of the cavity by $0.15a$. After the reactive ion etching step that transfers the holes forming the photonic crystal into the GaAs waveguide structure, we established an Ohmic back contact to the buried n+ layers and defined 300 μm × 400 μm photodiode mesas using photolithography and wet etching techniques. Within the 200 μm × 200 μm windows that were opened in the metallic top contact for optical access we established an array of 5 × 5 photonic crystals. Finally, suspended photonic crystal membrane structures were fabricated by selectively removing the $Al_{0.8}Ga_{0.2}As$ layer beneath the GaAs waveguide core to leave a free-standing, p–i–n-doped GaAs membrane.

The established contacts enable us to realize an axial electric field that can be tuned by varying the voltage applied across the p–i–n junction (V_{app}). Figure 9.8c shows a typical current–voltage trace recorded without illumination at $T = 15$ K. Clear rectifying behaviour is observed with a forward bias current onset of $V_{bi} \sim 1.1$ V, corresponding to the built-in potential in the membrane p–i–n diode, and negligible current flow (< 0.01 μAcm^{-2}) in reverse bias. From the built-in potential and the device geometry, we estimate the static electric field to be $F = (V_{bi}–V_{app})/d$, where $d = 110$ nm is the thickness of the intrinsic region and V_{app} is the applied electrostatic potential. Thus, we expect that static electric fields in the range 0 kVcm^{-1} < $|F|$ < 100 kVcm^{-1} can be applied parallel to the QD-growth axis, as depicted in Fig. 9.8a inset.

The sample was mounted in a liquid He-flow cryostat and cooled down to $T = 15$ K. For excitation, we used a pulsed Ti:sapphire laser ($f_{laser} = 80$ MHz, 2 ps duration pulses) tuned into resonance with a higher energy cavity mode (1.305 eV < E_{laser} < 1.355 eV) in order to excite QDs located inside the cavity only. The QD micro-PL was collected via a 100× microscope objective (numerical aperture = 0.5) providing a spatial resolution of < 1 μm and the signal was spectrally analysed by a 0.55 m imaging monochromator and detected with a Si- or an InGaAs-based, liquid nitrogen cooled charge coupled device detector. For time-resolved measurements, we used a fast silicon avalanche photodiode that provided a temporal resolution < 100 ps after deconvolution.

A typical PL spectrum of a single QD-cavity system in the weak coupling regime is presented in Fig. 9.9a. The strong emission line highlighted with

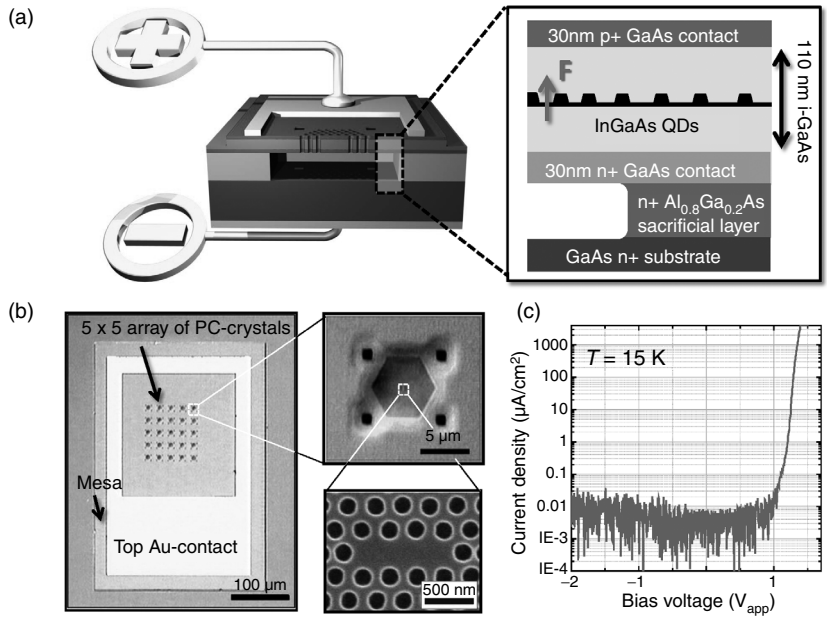

9.8 Electrically tunable single-QD PC nanocavities investigated. (a) Schematic cross-sectional representation of the device and layer sequence of the active region. The polarity of the static electric field (F) is indicated. (b) Microscope image of one of the diode windows showing the 5 × 5 array of PCs and image of higher magnification depicting a single PC. The scanning electron microscope image shows one of the L3 cavities at the centre of each PC. (c) Current-voltage characteristic of the device recorded without illumination. (Source: Adapted from Laucht *et al.* (2009b).)

the shaded area on the left-hand side stems from the cavity mode emission and is, in this particular case, strongly detuned (ΔE = 15 meV) from the discrete QD emission lines. The latter can be distinguished into *s*-shell and *p*-shell transitions according to the corresponding occupation of the QD. Here, the strong and well-separated emission line labelled *X* (highlighted with the shaded area on the right-hand side of the figure) was shown to stem from the single exciton transition by conducting excitation power dependent PL spectroscopy ($I \propto P^m$ with $m = 0.95$, data not shown).

Although no discrete QD transitions are present in the spectral vicinity of the cavity mode, pronounced PL emission is still observed from the cavity mode. For this system we conducted photon cross-correlation measurements between the cavity mode and the QD single exciton transition, which were detuned one from the other by $\Delta E > 18$ meV. The excitation power for the experiment was chosen just below saturation of the single exciton line. In Fig. 9.9b we plot the cross-correlation histogram as a function of

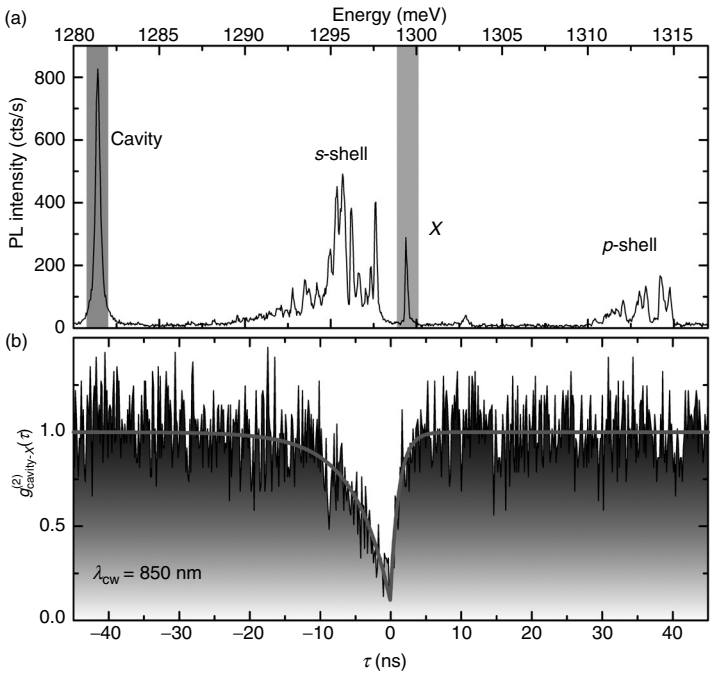

9.9 (a) PL spectrum of a QD-cavity system with the cavity mode detuned to ΔE = 18 meV lower energy than the single exciton transition. (b) Cross-correlation histogram between the cavity mode and the single exciton. Here, $\tau > 0$ corresponds to detection of a photon from the single exciton upon detection of a photon from the cavity mode. The solid line is a fit to the data. (Source: Adapted from Laucht *et al.* (2011).)

the time between two detection events. Here, $\tau > 0$ corresponds to detection of a photon from the exciton after detection of a photon from the cavity mode. At zero time delay ($\tau = 0$ ns) we observe a clear dip in the histogram. A fit to the data yields $g^{(2)}_{\text{cavity}-X}(0) = 0.11$ after deconvolution, showing the very high degree of anti-correlated emission from the cavity mode and the investigated single exciton line, and evidences that this cavity mode is predominantly fed by only this one QD. Similar experiments have been published by Hennessy *et al.* (2007), Kaniber *et al.* (2008), Winger *et al.* (2009) and are also presented by Tarel *et al.* in the next chapter where similar results to our Fig. 9.9 are presented.

Although phonon-mediated feeding of the cavity mode has already been demonstrated by, for example, Hohenester *et al.* (2009) to be effective for small dot-mode detunings $\Delta E < 5$ meV, the cross-correlation measurement clearly suggests the existence of an additional mechanism that non-resonantly feeds photons into the cavity mode for much larger detunings. In the past few years this scenario has been corroborated and validated by Hennessy

et al. (2007), Press *et al.* (2007), Kaniber *et al.* (2008) and Winger *et al.* (2009). Strong support for the multi-exciton feeding of the cavity mode is obtained by conducting time-resolved PL measurements when the QD-cavity system is excited above saturation of the *s*-shell levels (P = 250 nW for our excitation conditions).

We plot the time-resolved emission intensity of a QD-cavity system in Fig. 9.10a, as a function of the wavelength. Emission from the *p*-shell transitions of QD1 ($\lambda_{p-\text{shell1}}$ = 930–935 nm) and QD2 ($\lambda_{p-\text{shell2}}$ = 943–948 nm) occurs rapidly after the arrival of the laser excitation pulse and decays within a few nanoseconds. Emission from the *s*-shell transitions of QD1 ($\lambda_{s-\text{shell1}}$ = 940–945 nm) and QD2 ($\lambda_{s-\text{shell2}}$ = 962–967 nm) is temporally delayed, such that the maximum intensity is not reached until ~4–6 ns after excitation.

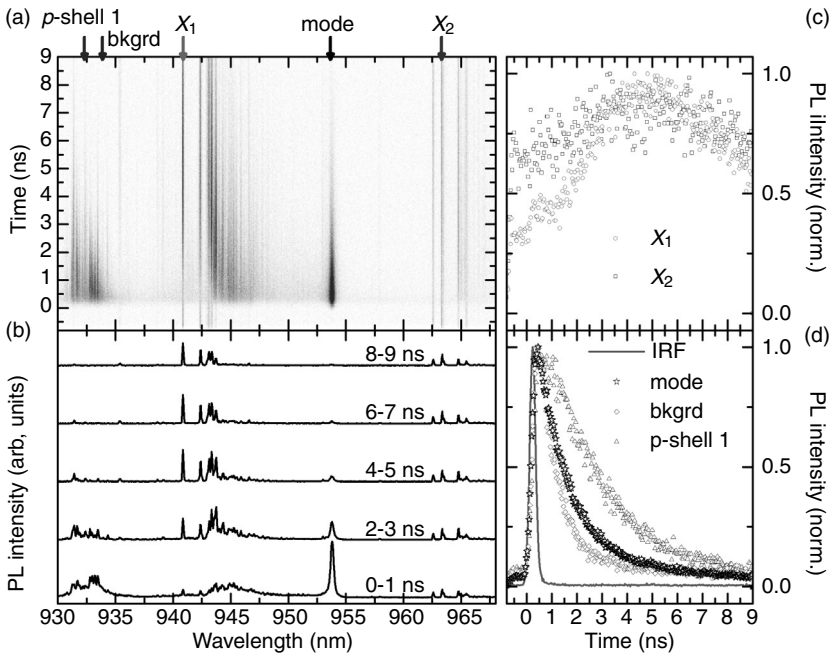

9.10 (a) Contour plot of the time-resolved PL intensity of a QD-cavity system as a function of emission wavelength. (The spectrally broad mode emission at early times is an artefact of plotting and not a physical effect.) Here, the linear grey scale was chosen such that features of low intensity are very visible and the intensity above a certain threshold is plotted with the same shade of grey. (b) PL spectra at different time delays after the laser pulse, each integrated over 1 ns. (c) and (d) Extracted, normalized PL intensity for (c) X_1 (circles) and X_2 (rectangles) and (d) cavity mode (stars), *p*-shell 1 (triangles), and *p*-shell 1 background (diamonds) as a function of time delay after the laser pulse. The IRF is plotted as solid line. (Source: Adapted from Laucht *et al.* (2010).)

At that time the population in the dot has already decayed to the single exciton level. Emission prior to the arrival of the laser pulse at 0 ns originates from excitation due to the previous excitation cycle, 12.5 ns earlier. The emission from the cavity mode at λ_{cav} = 954 nm occurs rapidly after arrival of the excitation pulse and decays quickly within ~2 ns. The spectra plotted in Fig. 9.10b show again the time evolution of the whole QD-cavity system. Here, we integrated the measured PL signal over Δt = 1 ns time intervals and present the resulting spectra for the time intervals from 0–1, 2–3, 4–5, 6–7 and 8–9 ns, from bottom to top in Fig. 9.10b. For the first time interval, emission from the *p*-shell states of QD1 and QD2 and from the cavity mode dominates the spectrum. However, the intensity of this emission decreases rapidly and vanishes almost completely by 5 ns after the excitation. The dominating peaks of the spectrum are now the *s*-shell emission of QD1 and QD2, whilst hardly any signal from the according *p*-shells or the cavity mode is observed.

For a more quantitative comparison, we plot the integrated, normalized PL intensity of X1 (circles) and X2 (rectangles) in Fig. 9.10c, and of mode (stars), *p*-shell1 (triangles) and *p*-shell background emission (diamonds) in Fig. 9.10d. The solid line is the instrument response function (IRF) of our experimental setup, measured with the spectral detection window tuned to the laser wavelength. It serves as reference for the time when the laser pulse excites the sample and allows us to determine the zero point of the time axis. While emission from the cavity mode, *p*-shell states and *p*-shell background occurs immediately after the laser pulse, the emission from the single excitons X1 and X2 is delayed and is temporally completely uncorrelated with the mode emission. It is also interesting to take a closer look at the decay times. The cavity mode decays (τ_{mode} = 1.4±0.1 ns) even faster than the selected discrete *p*-shell state ($\tau_{p\text{-shell1}}$ = 2.2±0.1 ns), but slower than the *p*-shell background between the discrete emission lines (τ_{bkgrd} = 0.8±0.1 ns). Thus, feeding of the cavity mode apparently occurs from many different multi-exciton states as well as from the broad background arising from many particle exchange correlations, present at higher excitation levels (Dekel *et al.*, 1998).

We will continue to present our observation of SC, but to place it in its proper context, we first complete the theoretical description to consider the possible effect of higher rungs of the JC ladder and a component that will turn out to be crucial in our case, namely, pure dephasing.

9.5 Luminescence spectra in the nonlinear regime

Let us return to Fig. 9.3 where we left the discussion at the vanishing pumping case of the Jaynes–Cummings system, leading to the linear model. Increasing pumping, we leave the linear regime to enter lasing, a regime

and concept (of a 'microlaser' or 'one-atom laser') first introduced by Mu and Savage (1992) and later developed by Löffler *et al*. (1997), Benson and Yamamoto (1999), Karlovich and Kilin (2001) and Gartner (2011), among others. In this regime, the system grows a coherent optical field by injection of photons in the cavity from the QD. This is achieved with an inverted QD and results in a plateau at unity for $g^{(2)}(0)$, showing that the field has Poissonian fluctuations. In this case, studied by del Valle and Laussy (2010b, 2011), the system can be described semi-classically rather than at the full quantum level, which is not tractable for such large numbers of photons (culminating at about 50 for the parameters of Fig. 9.3). The approximation in Equation [9.13] becomes better with increasing number of photons. In Fig. 9.3a, we extended the approximation beyond its regime of validity to show where the system is properly described as a laser. Increasing pumping even more, the coherence brought by lasing is disrupted by the decoherence from the pumping and the system enters a third regime of self-quenching, with a collapse of cavity population, saturation of the QD to its excited state (being prevented by too large pumping to enter the SC Rabi oscillation) and thermal, or more appropriately, chaotic statistics in particle number fluctuations. This regime is well described by approximation of thermal fields.

Quenching has not been experimentally observed yet, possibly because the single two-level system picture applies less or even breaks down in this very high excitation regime. Theoretically, a more refined cothermal representation for the field (a convolution of thermal and coherent fields in the Glauber *P* representation) covers very well all regimes over the entire range of excitation. The approximations have, on the other hand, the advantage of separating the three regimes on clear physical grounds. However, perhaps the more interesting region is not covered in any of these classifications. This is the one that occurs between the linear (but quantum) and lasing (classical) regimes. For this reason we shall call it the '*nonlinear quantum regime*'. This is the case when a few manifolds – more than the first but not as many as to loose discretization due to quantization – are excited. Populating the second rung is the first such genuinely quantum case. Despite remarkable advances in recent years in reaching SC, there still lacks a direct observation in the PL of this fundamental deviation from the classical realm. With coherent excitation, on the other hand, strong indirect evidence has been reported, notably by Faraon *et al*. (2008) demonstrating photon blockade and by Kasprzak *et al*. (2010) using four-wave mixing.

A selection of representative spectral shapes in this regime is shown in Fig. 9.11, for three different cavity decay rates: $\gamma_a/g = 0.1$ as representative of exceedingly good systems, available in the near future for semiconductors and already reached in circuit QED; $\gamma_a/g = 0.5$ representative of state-of-the-art system, such as those reported by Ohta *et al*. (2011); and $\gamma_a/g = 1.15$, the case of our own experiment. In all cases, we assumed

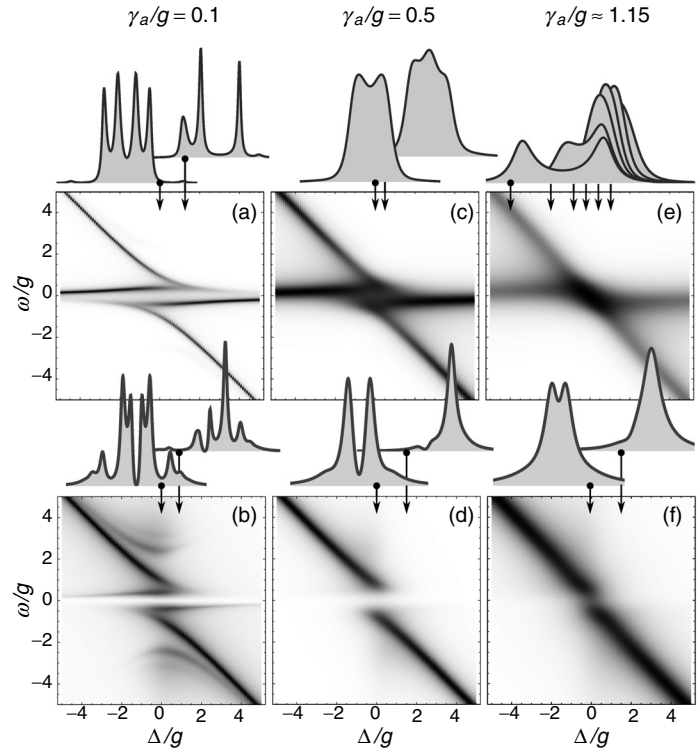

9.11 Typical spectral shapes for cavity (upper row) and QD (lower row) emission, for three cavity quality factors: better than is currently available in the first column ($\gamma_a/g \approx 0.1$), state-of-the-art in the second column ($\gamma_a/g \approx 0.5$), and for our experiment in third column ($\gamma_a/g \approx 1.15$). In all cases, ($\gamma_\sigma/g \approx 0.00334$). In the best system, the nonlinear JC transitions of Fig. 9.1b are well reproduced, particularly in the dot emission, which is, however, more difficult to detect. In the intermediate system, the large broadening of the higher rungs limits the observation to a mere doublet at resonance that collapses to a single line (that may narrow upon further increasing of pumping). Close to resonance, the nonlinear transitions are revealed and manifest as a triplet. For our system, an apparent crossing is observed when increasing pumping, with notable features such as persistence of coupling at large detuning too weak to be discriminated in an actual experiment.

$\gamma_\sigma/g = 0.00334$, a parameter also taken from our experiment. Beyond the linear regime, there is no longer the symmetry in cavity and exciton emission, and spectra differ considerably depending on the channel of detection. There are also variations owing to the effective quantum state realized in the system but for brevity we shall consider excitonic pumping only, which provides a reasonably comprehensive picture. Cavity PL spectra are shown on the upper row (a, c, e) and QD spectra on the lower row

(b, d, f) of Fig. 9.11 as density plots with cuts highlighted for a few detunings of interest (including resonance in all cases). The simplest expectation is that these figures should reconstruct Fig. 9.1b, which is partly the case at least for the best system. We see here that the QD emission features both the inner and the outer peaks, whereas the cavity emission suppresses the outer ones, for the reasons explained when discussing transitions in the JC ladder, Equations [9.5]–[9.7]. It would therefore appear interesting to detect QD emission; however, this is technically more difficult: cavity emission is directional with intensity $\propto n_a\gamma_a$, a product of two large numbers, whereas QD emission is in a large solid angle with intensity $\propto n_\sigma\gamma_\sigma$, a product of two small numbers. On the cuts shown, one sees also that the QD emission has a richer spectral structure as compared to the cavity spectrum that, in a good system, is composed of Lorentzian lines at the JC transitions (but between same-branch type of polaritons only). At resonance, a 'fork' neatly shows the four transitions involving the first two rungs of the ladder. With lower quality systems, although the VRS is neatly resolved, increasing pumping to populate the higher manifolds quickly leads to large broadenings that smother the Rabi doublet. A typical case, where the coupling strength is about twice the decay rate, is shown in Fig. 9.11c and 9.11d. At resonance, only a doublet is observed, in contrast to the fork of the better system. The splitting of this doublet goes from the VRS to a single line, as further rungs pile up in between. In the case shown, the doublet is mainly due to transitions from higher rungs. Increasing pumping furthermore at this point may lead to lasing, with the single line narrowing, and $g^{(2)}(0)$ locking to unity. This transition, not shown here, has been reported by Nomura *et al*. (2010) and is one of the rare instances where the QD-microcavity system has been induced to climb the JC ladder under incoherent excitation.

But rather than following the lasing any further we note that there is still a clear deviation from the mere crossing scenario as is quite apparent from the density plot. One can track the apparition of spectral triplets close to – but not at – resonance. Straying from resonance pins the inner transitions away from one of the bare modes that is detuned away. At resonance, although SC is optimum, it conceals its features by a symmetry that detuning allows to break. In the counterpart for QD emission, a clear deviation of the PL shape from two Lorentzians is observed in the form of two elbows on the flank of two peculiarly shaped polariton lines. The elbows are due to the outer JC transitions while the shape of the polariton lines is due to an absorption line carved in an emerging structure. One sees the latter effect more clearly once again by detuning the system, with a hole carved at the cavity frequency. This hole is due to the onset of lasing, with the cavity sucking excitation from the QD. We will return to this point when discussing the lasing regime.

Turning to the last case, that of our own experimental system, with sufficiently small γ_a such as to display an unambiguous VRS, we observe that upon increasing pumping to populate the JC ladder, the Rabi splitting is quickly lost because of the very fast broadening at resonance. However, the system remains strongly coupled throughout. One piece of evidence for this is the shift of the cavity emission on both sides of the crossing, which tracks the polariton energy Equation [9.4] rather than the bare cavity. The lack of features at the expected anticrossing is shown by the various cuts around the resonance, each of them in isolation displaying no phenomenology that one could distinguish from WC. In an actual experiment, it is therefore difficult to reach any conclusion since both modes are anyway shifted with the control parameter that detunes one from the other. In the QD emission, the hole carving of lasing onset reduces to a kink and the Rabi doublet displays a splitting with fat tails.

In summary, there is a rich phenomenology associated with experimental observables when studying the strong-coupling regime with cavities containing QDs. However, much of it is technically difficult to access and, unless the system is of an exceedingly good quality, what remains is not sufficiently explicit to provide compelling evidence that one climbs the JC ladder. Other more mundane mechanisms can lead to similar phenomenology. We give one such example in the next section.

9.6 Effects of pure dephasing

'*Pure dephasing*' is a dephasing of the off-diagonal elements of the density matrix, a mechanism washing out the phase relationship between states without changing their population (the adjective 'pure' is required in some fields where the decay of population is also called dephasing; not fearing confusion, we will drop it in the following). As might be expected, it is extremely important in semiconductors, since the quantum states are typically in contact with reservoirs, couple to various degrees of freedom, etc. A major source of decoherence in QDs is due to coupling to the crystal lattice. At high temperatures, Borri *et al*. (2005) identified an exciton dephasing via interactions with phonons, while at high excitation powers, Favero *et al*. (2007) linked it to the fluctuating charge environment of the QD. In the master equation, this type of dephasing can be included with an additional Lindblad term $L_\phi\rho = \gamma_\phi(\sigma_z\rho\sigma_z - \rho)/4$ in Equation [9.2], with $\sigma_z = [\sigma^+, \sigma]$. This term has been considered by Laucht *et al*. (2009a) and Auffèves *et al*. (2009) in the linear regime and by Gonzalez-Tudela *et al*. (2010a) and Auffèves *et al*. (2010) in the nonlinear regime. Other theoretical approaches have been pursued beyond this phenomenological model, for instance Kaer *et al*. (2010) considered non-Markovian effects. Dephasing has a nontrivial and sometimes unexpected effect on the dynamics of light-matter coupling of

detuned systems, such has been discussed by Auffèves *et al.* (2009). However, we will focus on the case of resonance in the following.

In the linear regime, dephasing leads to a broadening of the polariton lines, and a collapse of the Rabi splitting. This added degree of freedom allows a remarkable fit of the experimental data in the sense that a global fit of all PL lines can be obtained with essentially constant system parameters (coupling strength and lifetime) and also fixed pumping strength-conditions that closely correspond to the experimental situation. This is shown in Fig. 9.12a, where we investigated the cavity PL spectrum as a function of temperature. Examples of the recorded spectra from Laucht *et al.* (2009a) are plotted on the figure for temperatures ranging from $T = 17.5$ to 48.1 K. The excitation power density used for these measurements was 10 W/cm^2, far below saturation of the exciton transition. Clearly, we resolve the two polariton peaks for $T < 30$ K, but they broaden rapidly between $T = 30$ and 40 K and merge into a single poorly resolved feature at higher temperatures. The entire detuning-dependent data at each fixed temperature was fitted by Laucht *et al.* (2009a) with parameters that are summarized in Fig. 9.12b. The temperature is not expected to influence either the decay or pumping rates

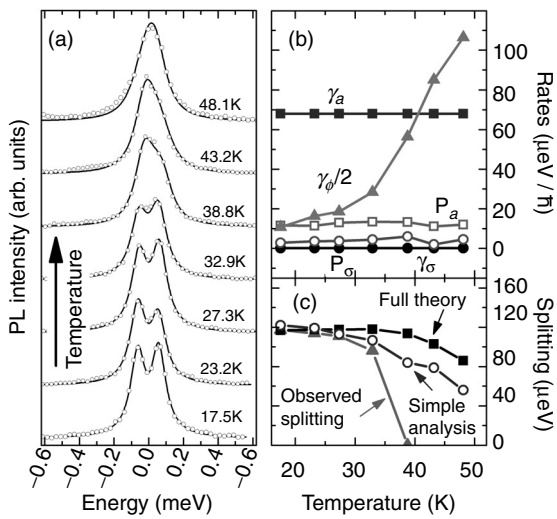

9.12 (a) Spectra of the exciton polaritons at resonance as a function of temperature. The circles correspond to experimental data, while the solid lines are fits to the theory. In (b), the fitting parameters are displayed as they change with increasing temperature. Panel (c) shows the theoretically expected Rabi splitting at resonance (filled squares), the one obtained from the fitting of the two Lorentzian peaks in the PL spectra (open circles), and the one obtained from the separation of the maxima of the two peaks (filled triangles). (Source: Adapted from Laucht *et al.* (2009a).)

of QD and cavity mode. This expectation is confirmed by the fitting, where $\gamma_{a,\sigma}$ were kept globally constant and $P_{a,\sigma}$ were *found* to remain constant as T varied. The only fitting parameter that varies appreciably with the temperature is the pure dephasing rate γ_ϕ (filled triangles in Fig. 9.12b) that increases linearly for $T < 30$ K with a temperature coefficient $\alpha_0 \sim 1.1$ μeV/K, and more rapidly for higher temperatures. The linear temperature dependence of the dephasing rate is strong evidence for decoherence mediated by coupling to acoustic phonons, along the scheme of Favero *et al*. (2003), Besombes *et al*. (2001) and Favero *et al*. (2007), who report temperature coefficients of the zero-phonon exciton transition in the range $\alpha_0 = 0.04$–4 μeV/K (see also the discussions by Borri *et al*. (2005) and Urbaszek *et al*. (2004) who concur with these conclusions).

In our experiment, therefore, the system does not climb the JC ladder, since it is foiled by dephasing. Instead, it remains in the first manifold. We also observed no line narrowing when losing the PL splitting with increasing excitation, supporting again this scenario. At the same time, we retain strong coupling throughout, as shown in Fig. 9.12c where we plot the Rabi splitting between the dressed states (filled squares), a quantity made available by the theory. The VRS is insensitive to the temperature for $T < 40$ K and reduces slightly at higher temperature. As discussed earlier, the VRS differs strongly from the observed splitting (filled triangles), which quickly collapses, a fact from which one should not infer that the system crossed to WC (although this could be the case as well, as reported by Münch *et al*. (2009)). In fact, a simpler analysis of the peak splitting made by fitting with two Lorentzians only (open circles), indeed confirms that in all cases, the observed singlet has an underlying structure other than that of WC. The quantitative disagreement with our theory is not too severe in this case but this procedure has no guarantee to provide accurate, or even meaningful, results in other cases. We also note that the cavity feeding mechanism, which we have studied and characterized in detail, helps in resolving the splitting. If we set $P_a = 0$ in the theory, we lose significantly in contrast (but not too much in splitting). Unfortunately, it is not so easy experimentally to control the effective quantum state of the system. These observations therefore underscore the need for a full theoretical description of the emission spectrum and its variation with detuning in order to specify if the system operates in the strong or WC regime, and to infer from the data accurate estimates of the system parameters.

In the quantum nonlinear regime, dephasing has a more striking manifestation: it collapses the inner peaks of the cavity PL (in a system good enough to observe them) into a single line, affecting the Rabi doublet or the outer peaks much more weakly, even though the latter are strongly suppressed anyway in the cavity spectrum, as discussed above. Inner transitions become degenerate, the system not being able anymore to distinguish

between the various branches. All the closely spaced transitions are then emitted at a common frequency, that of the cavity. As a result, a triplet is observed that keeps the VRS essentially untouched with a broader central line overlapping it. Qualitatively, the triplet due to dephasing of the JC nonlinearities is quite similar to the triplet that arises due to finite detuning as discussed above. In both cases quantum nonlinearities from higher rungs are involved, and as such a complex and interesting phenomenon is hiding behind a ubiquitous and moot spectral shape. Spectral triplets have been reported in the literature, first by Hennessy *et al*. (2007) and then by Ota *et al*. (2009a), but they have been explained as stemming from the first manifold, namely, as an incoherent superposition (i.e. at different times) of a conventional Rabi doublet on the one hand and the empty cavity on the other hand, the co-existence of these two regimes being probably due to, among other possible scenarios, fluctuating charges that bring the QD in and out of resonance. This is in stark contrast with the triplets we have presented above, even the one caused by dephasing, which require more than one excitation to access the higher rungs. In the QD direct emission, dephasing merely broadens the exciton linewidth while keeping the Rabi doublet (and other peaks if visible) with no change in the parity of the system, and as such behaves in a way more similar to the linear regime. Such an evolution is shown in Fig. 9.13 for both the cavity emission (right side) and QD direct emission (left side). It has been shown by Laussy *et al*. (2010) that spectral triplets due to dephasing and/or detuning are consistent with the experiment. However, it still remains to be proven which mechanism is actually accountable for the observed triplet emission. Beside checking QD emission, which we have already said is technically challenging, one could check for instance whether the central peak undergoes lasing, a feature it preserves when arising under SC. Unambiguous identification of the nature of the spectral triplets will become increasingly important if quantum nonlinearities, such as the Jaynes–Cummings fork, will remain absent from the collection of spectral shapes.

9.7 Lasing

Finally we turn to the case of lasing, of great interest for applications. A recent review is given by Strauf and Jahnke (2011) and the topic is also covered by Gies *et al*. in Chapter 3. The master equation is not the ideal toolbox to tackle this regime in the Jaynes–Cummings model where the system can accommodate a very large number of photons. This implies in turn an extremely large Hilbert space. When additional saturation effects of the QD from a more realistic semiconductor description are taken into account, lasing is tamed and the number of photon does not grow so efficiently. This allows, for state-of-the-art parameters, numerical solutions of

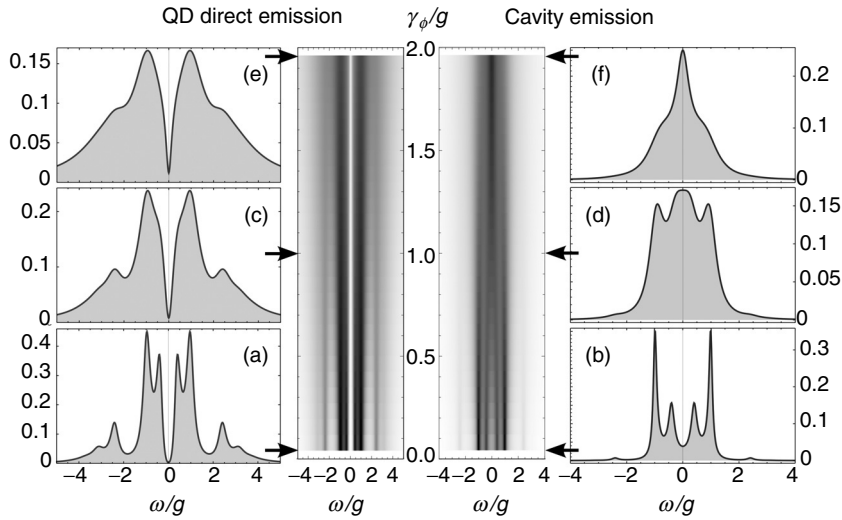

9.13 Density plots of QD (left) and cavity (right) PL spectra as a function of pure dephasing. A transition from JC quantum nonlinearities to a triplet is observed in the cavity emission. Keeping the value of $\gamma_\phi = g$ and increasing pumping, one would see a transition from the VRS to a spectral triplet, much like the observation of Ota *et al.* (2009b). In the cavity emission, dephasing collapses together the thinly spaced transitions of the higher JC rungs. Parameters are $\gamma_d/g \approx 0.1$ and γ_σ/g the value of our experiment.

von Neumann equations as shown by C. Gies *et al.* in this volume. In our pure Jaynes–Cummings case, one observes an interesting phenomenon of breakdown of the quantum regime, where a not too large number of quantum correlators of the type $\langle a^{\dagger m} a^n \sigma^{\dagger \mu} \sigma^\nu \rangle$ all assuming sizable values, evolve into a regime with a very large number of them assuming vanishingly small values, showing how the quantized field smooths out and becomes classical. This is an awkward situation when numerically addressing the problem as we do in the basis of dressed states, since the small values involved require one to go beyond machine precision arithmetic to keep track of this loss of granularity of the field.

This transition is shown in Fig. 9.14 where the cuts are shown in log scale to follow the transition from the quantum to the classical regime. At vanishing pumping (Fig. 9.14a), the PL spectrum is the VRS and consists of essentially two Lorentzians (the coupling strength being high enough in the case we have chosen). Increasing pumping but still keeping a small number of particles in the system, we populate the higher manifolds, leading to apparition of the JC nonlinear peaks (Fig. 9.14b). These are, again, better seen in the QD emission although all are neatly visible on the log scale. For exceedingly good systems, the field quantization can be tracked up to very high in

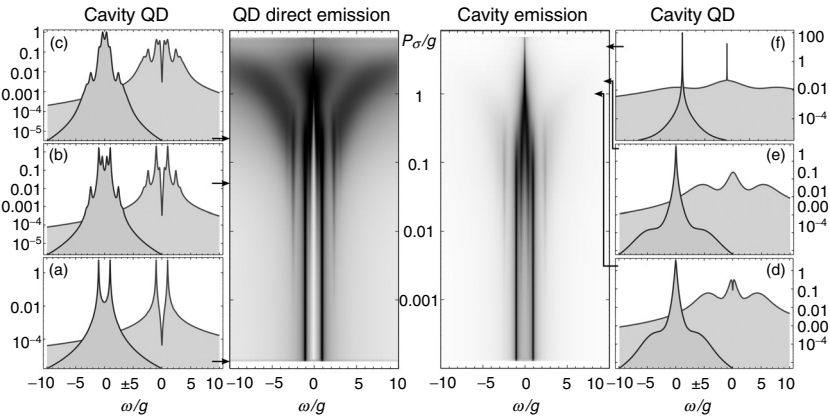

9.14 Cavity and QD PL spectra with increasing pumping of the QD. At vanishing pumping (a) the VRS is observed. Peaks from transitions higher in the JC ladder appear under small pumping (b) and start to melt when more numerous and overlapping as a result of climbing further the ladder (c). This leads to a new and simpler structure, a triplet (d) that features a sharp absorption line in the QD spectrum, due to a coherent scattering of excitation from the dot to the cavity field, which sucks excitation to build lasing. When coherence of the optical field is strong enough, the absorption peak disappears (e) and is followed by a scattering peak, the counterpart of Rayleigh scattering peak of the conventional Mollow triplet, caused by cavity photon of the now-coherent macroscopic field scattering on the QD. At this stage, the cavity is fully lasing and is a very narrow Lorentzian line.

the ladder, as shown by Laussy and del Valle (2009) for the case $\gamma_a/g = 0.01$ (where one can climb several dozens of rungs). Increasing pumping further, the peaks overlap and start to melt (Fig. 9.14c). The cavity, which favours the transitions close to its energy, quickly goes into lasing and gives rise to an intense central peak with a narrowing linewidth, as shown and described analytically by Poddubny *et al*. (2010). The QD, which equally favours inner and outer transitions, shows a stronger emission at the origin simply because two of the four transitions contribute there. The other two transitions form elbows on both sides, in the ratio 1:2. Still increasing pumping, one enters the lasing regime (Fig. 9.14d). The complicated PL spectrum featuring a plethora of peaks at anharmonic transitions of the JC ladder gives way to a structure of much reduced complexity: a triplet. This triplet is also different from the three variations we have encountered before. It is, in fact, straightforwardly recognizable as a variation of the celebrated Mollow (1969) triplet, which arises in the resonance fluorescence of an atomic system, that is, the PL of a two-level system on which impinges an intense laser field.

Here, there is no external laser driving the system, but the cavity field grows its own coherence under the action of SC and the QD effectively finds itself

bathed in a macroscopic, coherent field, exhibiting a phenomenology close to that of the conventional Mollow triplet. Differences are discussed in details by del Valle and Laussy (2010b); we will limit ourselves here to the most striking results: along with the excellent analytical approximations that exist in this regime for quantities such as n_a, as shown in Fig. 9.3, one can also derive an excellent approximation for the Mollow triplet lineshape formed under incoherent pumping, which becomes better and essentially exact as the number of photons is increased. This shows again that a classical or semi-classical picture emerges that adequately describes the system, getting rid of the irrelevant underlying quantum details such as the structure of the JC very high in the ladder. The formula is qualitatively very good for panels (d) and (e) of Fig. 9.14 and it is indistinguishable by eye from the computed result for panel (f), which features the triplet and a very narrow peak (the triplet is more apparent in linear scale). The small quantitative discord for panels (e) and (f) is due to the fact that the cavity has not yet fully formed coherence, which can be seen in two ways. The first one is that the cavity itself is not exactly Lorentzian, as in the fully formed case in panel (f). The second is more interesting: as the Mollow triplet forms, the space separating the two Rabi peaks at low pumping evolves into an absorption line, as seen in panel (d). This line becomes filled until a point where it disappears (e) and then appears again, this time positively, forming a narrow peak sitting on the triplet (f). The latter is the counterpart in our system of the Rayleigh peak of the conventional Mollow triplet, which is due to the atom elastically scattering photons from the laser. In our case, the photons are also, in the full sense of the term, elastically scattered by the QD, originating from the now coherent cavity field, strong enough to behave like an external field and factored out from the SC QD that built its coherence. In panel (Fig. 9.14d), when the system is still not fully grown as a classical and continuous field, the scattering is reversed; the cavity is resonantly sucking the excitation from the dot to build its coherent field, resulting in the negative δ peak. We witness in this process a beautiful self-consistent coherence build-up in a quantum system that evolves into a classical one.

9.8 Conclusions and future trends

Some results related to the young field of strong coupling of a QD in a microcavity have been discussed. In the wider context of cavity QED, the semiconductor implementation presents, at a fundamental level, a few specificities of its own, essentially, a noisy environment that brings extraneous sources of excitation and dephasing. Its coupling strength is small compared to decay rate of one bare mode, usually the cavity, but can greatly exceed the other mode, leading to peculiar interference effects. In this regime of few Rabi oscillations, one should pay particular attention to such details as which effective quantum state is realized in the system and through which channel of emission it is detected.

Doing so, an excellent quantitative agreement with all experiments that have been subjected to this analysis has been obtained. The field will be mature for applications when a deep understanding of the physics and complete control of experimental realizations has been achieved. We have shown that a qualitative description might be incorrect, with such configurations where an observed splitting in PL could be confused for a Rabi splitting or the other way around. At the same time, first results analysing PL have been very encouraging and suggest that semiconductors do implement a robust version of the fundamental Jaynes–Cummings Hamiltonian. So far the crowning achievements from the experimental point of view are the VRS, reported in late 2004, and the lasing in SC, reported in early 2010. Even these two milestones leave much room for further developments, such as control of the quantum state realized in the system, observation of the SC dynamics in the two complementary channels that are the cavity and direct QD emission, or, more interestingly, investigation of the branching between these two limits, with manifestation of new fundamental structures such as a new kind of Mollow triplet. The more interesting intermediate quantum regime where a few quanta undergo the SC dynamics still remains elusive. Puzzling phenomena have been reported in the form of spectral triplets. As the field progresses with a deeper control of the system parameters, schemes of excitation and methods of detection, more of the phase-space of weak and strong coupling will be explored and more of the spectral shapes that we have presented will surface.

9.9 Acknowledgements

The authors thank Professor Jahnke for editing this volume and for a careful reading of the manuscript, and F. P. Laussy thanks him for his invitation to discuss with P. Gartner, C. Gies and the rest of his group some of the results compiled here. We have benefited throughout the years from discussions with J. M. Villas-Bôas, D. Sanvitto, E. Cancellieri, M. Glazov, A. Poddubny, M. Schrapp, K. Müller and N. Hauke on this and related topics. DFG via SFB-631, the Nanosystems Initiative Munich project funded in the framework of the German excellence initiative, the Emmy Noether project HA 5593/1-1, MEC (MAT200801555/NAN, QOIT-CSD2006-00019), CAM (S-0505/ESP-0200), the Newton International fellowships program, the Alexander von Humboldt Foundation and EU FP-7 via SOLID and Marie Curie Initiative 'SQOD' are acknowledged for funding.

9.10 References

Agarwal, G. S. and R. R. Puri. Exact quantum-electrodynamics results for scattering, emission, and absorption from a Rydberg atom in a cavity with arbitrary Q. *Phys. Rev. A*, **33**:1757, 1986.

Andreani, L. C., G. Panzarini, and J.-M. Gérard. Strong-coupling regime for quantum boxes in pillar microcavities: Theory. *Phys. Rev. B*, 60:13276, 1999.

Aoki, T., B. Dayan, E. Wilcut, W. P. Bowen, A. S. Parkins, T. J. Kippenberg, K. J. Vahala, and H. J. Kimble. Observation of strong coupling between one atom and a monolithic microresonator. *Nature*, **443**:671, 2006.

Astafiev, O., K. Inomata, A. O. Niskanen, T. Yamamoto, Yu. A. Pashkin, Y. Nakamura, and J. S. Tsai. Single artificial-atom lasing. *Nature*, **449**:588, 2007.

Auffèves, A., J.-M. Gérard, and J.-P. Poizat. Pure emitter dephasing: A resource for advanced solid-state single-photon sources. *Phys. Rev. A*, **79**:053838, 2009.

Auffèves, A., D. Gerace, J.-M. Gérard, and J.-P. Poizat. Controlling the dynamics of a coupled atom-cavity system by pure dephasing. *Phys. Rev. B*, **81**:245419, 2010.

Averkiev, N.S., M.M. Glazov, and A.N. Poddubny. Collective modes of quantum dot ensembles in microcavities. *Sov. Phys. JETP*, **135**:959, 2009.

Benson, O. and Y. Yamamoto. Master-equation model of a single-quantum-dot microsphere laser. *Phys. Rev. A*, **59**:4756, 1999.

Besombes, L., K. Kheng, L. Marsal, and H. Mariette. Acoustic phonon broadening mechanism in single quantum dot emission. *Phys. Rev. B*, **63**:155307, 2001.

Borri, P., W. Langbein, U. Woggon, V. Stavarache, D. Reuter, and A. D. Wieck. Exciton dephasing via phonon interactions in InAs quantum dots: Dependence on quantum confinement. *Phys. Rev. B*, **71**:115328, 2005.

Carmele, A., M. Richter, W. W. Chow, and A. Knorr. Antibunching of thermal radiation by a room-temperature phonon bath: A numerically solvable model for a strongly interacting light-matter-reservoir system. *Phys. Rev. Lett*., **104**:156801, 2010.

Carmichael, H. J., R. J. Brecha, M. G. Raizen, H. J. Kimble, and P. R. Rice. Subnatural linewidth averaging for coupled atomic and cavity-mode oscillators. *Phys. Rev. A*, **40**: 5516, 1989.

Cui, G. and M. G. Raymer. Emission spectra and quantum efficiency of single-photon sources in the cavity-QED strong-coupling regime. *Phys. Rev. A*, **73**:053807, 2006.

Dekel, E., D. Gershoni, E. Ehrenfreund, D. Spektor, J. M. Garcia, and P. M. Petroff. Multiexciton spectroscopy of a single self-assembled quantum dot. *Phys. Rev. Lett*., **80**:4991, 1998.

del Valle, E. *Microcavity quantum electrodynamics*. VDM Verlag, 2010.

del Valle, E. and F. P. Laussy. Effective cavity pumping from weakly coupled quantum dots. *Superlatt. Microstruct*., **49**:241, 2010a.

del Valle, E. and F. P. Laussy. Mollow triplet under incoherent pumping. *Phys. Rev. Lett*., **105**:233601, 2010b.

del Valle, E. and F. P. Laussy. Regimes of strong light-matter coupling under incoherent excitation. *Phys. Rev. A*, **84**, 043816, 2011.

del Valle, E., F. P. Laussy, and C. Tejedor. Luminescence spectra of quantum dots in microcavities. II. Fermions. *Phys. Rev. B*, **79**:235326, 2009.

del Valle, E., S. Zippilli, F. P. Laussy, A. Gonzalez-Tudela, G. Morigi, and C. Tejedor. Two-photon lasing by a single quantum dot in a high-Q microcavity. *Phys. Rev. B*, **81**:035302, 2010.

Faraon, A., I. Fushman, D. Englund, N. Stoltz, P. Petroff, and J. Vuckovic. Coherent generation of non-classical light on a chip via photon-induced tunnelling and blockade. *Nat. Phys*., **4**:859, 2008.

Favero, I., G. Cassabois, R. Ferreira, D. Darson, C. Voisin, J. Tignon, C. Delalande, G. Bastard, Ph. Roussignol, and J.-M. Gérard. Acoustic phonon sidebands in the emission line of single InAs/GaAs quantum dots. *Phys. Rev. B*, **68**:233301, 2003.

Favero, I., A. Berthelot, G. Cassabois, C. Voisin, C. Delalande, Ph. Roussignol, R. Ferreira, and J.-M. Gérard. Temperature dependence of the zero-phonon linewidth in quantum dots: An effect of the fluctuating environment. *Phys. Rev. B*, **75**:073308, 2007.

Gartner, P. The two-level atom laser: Analytical results and the laser transition. *Phys. Rev. A*, **84**:053804, 2011.

Gies, C., J. Wiersig, M. Lorke, and F. Jahnke. Semiconductor model for quantum-dot based microcavity lasers. *Phys. Rev. A*, **75**:013803, 2007.

Gonzalez-Tudela, A., E. del Valle, E. Cancellieri, C. Tejedor, D. Sanvitto, and F. P. Laussy. Effect of pure dephasing on the Jaynes-Cummings nonlinearities. *Opt. Express*, **18**:7002, 2010a.

Gonzalez-Tudela, A., E. del Valle, C. Tejedor, and F.P. Laussy. Anticrossing in the PL spectrum of light–matter coupling under incoherent continuous pumping. *Superlatt. Microstruct*., 47:16, 2010b.

Haroche, S. and D. Kleppner. Cavity quantum electrodynamics. *Phys. Today*, **42**:24, 1989.

Haug, H. and S. W. Koch. *Quantum theory of the optical and electronic properties of semiconductors*. World Scientific, 1990.

Hennessy, K., A. Badolato, M. Winger, D. Gerace, M. Atature, S. Gulde, S. Felt, E. L. Hu, and A. Imamoglu. Quantum nature of a strongly coupled single quantum dot–cavity system. *Nature*, **445**:896, 2007.

Hohenester, U., A. Laucht, M. Kaniber, N. Hauke, Andre Neumann, A. Mohtashami, M. Seliger, M. Bichler, and J. J. Finley. Phonon-assisted transitions from quantum dot excitons to cavity photons. *Phys. Rev. B*, **80**:201311(R), 2009.

Imamoglu, A. and R. J. Ram. Quantum dynamics of exciton lasers. *Phys. Lett. A*, **214**:193, 1996.

Jaynes, E.T. and F.W. Cummings. Comparison of quantum and semiclassical radiation theory with application to the beam maser. *Proc. IEEE*, **51**:89, 1963.

Kaer, P., T. R. Nielsen, P. Lodahl, A.-P. Jauho, and J. Mork. Non-Markovian model of photon-assisted dephasing by electron-phonon interactions in a coupled quantum-dot-cavity system. *Phys. Rev. Lett*., **104**:157401, 2010.

Kaniber, M., A. Laucht, A. Neumann, J. M. Villas-Bôas, M. Bichler, M.-C. Amann, and J. J. Finley. Investigation of the nonresonant dot-cavity coupling in two-dimensional photonic crystal nanocavities. *Phys. Rev. B*, **77**:161303(R), 2008.

Karlovich, T. B. and S. Y. Kilin. Quantum statistical properties of one-atom lasers. *Opt. Spectrosc*., **91**:343, 2001.

Kasprzak, J., S. Reitzenstein, E. A. Muljarov, C. Kistner, C. Schneider, M. Strauss, S. Höfling, A. Forchel, and W. Langbein. Up on the Jaynes-Cummings ladder of a quantum-dot/microcavity system. *Nat. Mater*., **9**:304, 2010.

Kavokin, A., J. J. Baumberg, G. Malpuech, and F. P. Laussy. *Microcavities*. Oxford University Press, 2011.

Khitrova, G., H. M. Gibbs, M. Kira, S. W. Koch, and A. Scherer. Vacuum Rabi splitting in semiconductors. *Nat. Phys*., **2**:81, 2006.

Kira, M. and S. W. Koch. Cluster-expansion representation in quantum optics. *Phys. Rev. A*, **78**:022102, 2008.

Laucht, A., N. Hauke, J. M. Villas-Bôas, F. Hofbauer, G. Böhm, M. Kaniber, and J. J. Finley. Dephasing of exciton polaritons in photoexcited InGaAs quantum dots in GaAs nanocavities. *Phys. Rev. Lett*., **103**:087405, 2009a.

Laucht, A., F. Hofbauer, N. Hauke, J. Angele, S. Stobbe, M. Kaniber, G. Böhm, P. Lodahl, M.-C. Amann, and J. J. Finley. Electrical control of spontaneous emission and strong coupling for a single quantum dot. *New J. Phys*., **11**:023034, 2009b.

Laucht, A., M. Kaniber, A. Mohtashami, N. Hauke, M. Bichler, and J. J. Finley. Temporal monitoring of non-resonant feeding of semiconductor nanocavity modes by quantum dot multiexciton transitions. *Phys. Rev. B*, **81**:241302(R), 2010.

Laucht, A., N. Hauke, A. Neumann, T. Günthner, F. Hofbauer, A. Mohtashami, K. Müller, G. Böhm, M. Bichler, M.-C. Amann, M. Kaniber, and J. J. Finley. Non-resonant feeding of photonic crystal nanocavity modes by quantum dots. *J. Appl. Phys*., **109**:102404, 2011.

Laussy, F. P. and E. del Valle. Optical spectra of the Jaynes-Cummings ladder. *AIP Conf. Proc.*, **1147**:46, 2009.

Laussy, F. P. and E. del Valle. On the spectroscopy of quantum dots in microcavities. *J. Phys.: Conf. Ser*., **210**:012018, 2010.

Laussy, F. P., G. Malpuech, A. Kavokin, and P. Bigenwald. Spontaneous coherence buildup in a polariton laser. *Phys. Rev. Lett*., **93**:016402, 2004.

Laussy, F. P., M. M. Glazov, A. Kavokin, D. M. Whittaker, and G. Malpuech. Statistics of excitons in quantum dots and their effect on the optical emission spectra of microcavities. *Phys. Rev. B*, **73**:115343, 2006.

Laussy, F. P., E. del Valle, and C. Tejedor. Strong coupling of quantum dots in microcavities. *Phys. Rev. Lett*., **101**:083601, 2008.

Laussy, F. P., E. del Valle, and C. Tejedor. Luminescence spectra of quantum dots in microcavities. I. Bosons. *Phys. Rev. B*, **79**:235325, 2009.

Laussy, F. P., E. del Valle, A. Gonzalez-Tudela, E. Cancellieri, D. Sanvitto, and C. Tejedor. Linear and nonlinear coupling of quantum dots in microcavities. *Int. Symp. Nanostr. Phys. Technol.*, **18**:298, 2010.

Laussy, F. P., A. Laucht, E. del Valle, J. J. Finley and J. M. Villas-Bôas, Luminescence spectra of quantum dots in microcavities. III. Multiple quantum dots. *Phys. Rev. B*., **84**:195313, 2011.

Löffler, M., G. M. Meyer, and H. Walther. Spectral properties of the one-atom laser. *Phys. Rev. A*, **55**:3923, 1997.

Mollow, B. R. Power spectrum of light scattered by two-level systems. *Phys. Rev*., **188**:1969, 1969.

Mu, Y. and C. M. Savage. One-atom lasers. *Phys. Rev. A*, **46**:5944, 1992.

Münch, S., S. Reitzenstein, P. Franeck, A. Löffler, T. Heindel, S. Höfling, L. Worschech, and A. Forchel. The role of optical excitation power on the emission spectra of a strongly coupled quantum dot-micropillar system. *Opt. Express*, **17**:12821, 2009.

Naesby, A., T. Suhr, P. T. Kristensen, and J. Mork. Influence of pure dephasing on emission spectra from single photon sources. *Phys. Rev. A*, **78**:045802, 2008.

Nomura, M., N. Kumagai, S. Iwamoto, Y. Ota, and Y. Arakawa. Laser oscillation in a strongly coupled single-quantum-dot–nanocavity system. *Nat. Phys*., **6**:279, 2010.

Ohta, R., Y. Ota, M. Nomura, N. Kumagai, S. Ishida, S. Iwamoto and Y. Arakawa, Strong coupling between a photonic crystal nanobeam cavity and a single quantum dot. *Appl. Phys. Lett*., **98**:173104, 2011.

Ota, Y., N. Kumagai, S. Ohkouchi, M. Shirane, M. Nomura, S. Ishida, S. Iwamoto, S. Yorozu, and Y. Arakawa. Investigation of the spectral triplet in strongly coupled quantum dot–nanocavity system. *Appl. Phys. Express*, **2**:122301, 2009a.

Ota, Y., M. Shirane, M. Nomura, N. Kumagai, S. Ishida, S. Iwamoto, S. Yorozu, and Y. Arakawa. Vacuum Rabi splitting with a single quantum dot embedded in a H1 photonic crystal nanocavity. *Appl. Phys. Lett*., **94**:033102, 2009b.

Perea, J. I., D. Porras, and C. Tejedor. Dynamics of the excitations of a quantum dot in a microcavity. *Phys. Rev. B*, **70**:115304, 2004.

Peter, E., P. Senellart, D. Martrou, A. Lemaitre, J. Hours, J. M. Gérard, and J. Bloch. Exciton-photon strong-coupling regime for a single quantum dot embedded in a microcavity. *Phys. Rev. Lett*., **95**:067401, 2005.

Poddubny, A. N., M. M. Glazov, and N. S. Averkiev. Nonlinear emission spectra of quantum dots strongly coupled to a photonic mode. *Phys. Rev. B*, **82**:205330, 2010.

Porras, D. and C. Tejedor. Linewidth of a polariton laser: Theoretical analysis of self-interaction effects. *Phys. Rev. B*, **67**:161310(R), 2003.

Press, D., S. Götzinger, S. Reitzenstein, C. Hofmann, A. Löffler, M. Kamp, A. Forchel, and Y. Yamamoto. Photon antibunching from a single quantum dot-microcavity system in the strong coupling regime. *Phys. Rev. Lett*., **98**:117402, 2007.

Raizen, M. G., R. J. Thompson, R. J. Brecha, H. J. Kimble, and H. J. Carmichael. Normal-mode splitting and linewidth averaging for two-state atoms in an optical cavity. *Phys. Rev. Lett*., **63**:240, 1989.

Reithmaier, J. P., G. Sek, A. Löffler, C. Hofmann, S. Kuhn, S. Reitzenstein, L. V. Keldysh, V. D. Kulakovskii, T. L. Reinecker, and A. Forchel. Strong coupling in a single quantum dot–semiconductor microcavity system. *Nature*, **432**:197, 2004.

Richter, M., A. Carmele, A. Sitek, and A. Knorr. Few-photon model of the optical emission of semiconductor quantum dots. *Phys. Rev. Lett*., **103**:087407, 2009.

Ritter, S., P. Gartner, C. Gies, and F. Jahnke. Emission properties and photon statistics of a single quantum dot laser. *Opt. Express*, **18**:9909, 2010.

Rubo, Y. G., F. P. Laussy, G. Malpuech, A. Kavokin, and P. Bigenwald. Dynamical theory of polariton amplifiers. *Phys. Rev. Lett*., **91**:156403, 2003.

Sanchez-Mondragon, J. J., N. B. Narozhny, and J. H. Eberly. Theory of spontaneous emission line shape in an ideal cavity. *Phys. Rev. Lett*., **51**:550, 1983.

Shore, B. W. and P. L. Knight. The Jaynes-Cummings model. *J. Mod. Opt*., **40**:1195, 1993.

Strauf, S. and F. Jahnke. Single quantum dot nanolaser. *Laser Photon. Rev*., **5**:607–633, 2011.

Thompson, R. J., G. Rempe, and H. J. Kimble. Observation of normal-mode splitting for an atom in an optical cavity. *Phys. Rev. Lett*., **68**:1132, 1992.

Urbaszek, B., E. J. McGhee, M. Krüger, R. J. Warburton, K. Karrai, T. Amand, B. D. Geradot, P. M. Petroff, and J. M. Garcia. Temperature dependent linewidth of charged excitons in semiconductor quantum dots: Strongly broadened ground state transitions due to acoustic phonon scattering. *Phys. Rev. B*, **69**:035304, 2004.

Wallraff, A., D. I. Schuster, A. Blais, L. Frunzio, R.-S. Huang, J. Majer, S. Kumar, S. M. Girvin, and R. J. Schoelkopf. Strong coupling of a single photon to a superconducting qubit using circuit quantum electrodynamics. *Nature*, **431**:162, 2004.

Weisbuch, C., M. Nishioka, A. Ishikawa, and Y. Arakawa. Observation of the coupled exciton-photon mode splitting in a semiconductor quantum microcavity. *Phys. Rev. Lett*., **69**:3314, 1992.

Wiersig, J. Microscopic theory of first-order coherence in microcavity lasers based on semiconductor quantum dots. *Phys. Rev. B*, **82**:155320, 2010.

Winger, M., T. Volz, G. Tarel, S. Portolan, A. Badolato, K. J. Hennessy, E. L. Hu, A. Beveratos, J. J. Finley, V. Savona, and A. Imamoglu. Explanation of photon correlations in the far-off-resonance optical emission from a quantum-dot – cavity system. *Phys. Rev. Lett*., **103**:207403, 2009.

Yamaguchi, M., T. Asano, K. Kojima, and S. Noda. Quantum electrodynamics of a nanocavity coupled with exciton complexes in a quantum dot. *Phys. Rev. B*, **80**:155326, 2009.

Yao, P., P. K. Pathak, E. Illes, S. Hughes, S. Munch, S. Reitzenstein, P. Franeck, A. Loffer, T. Heindel, S. Höfling, L. Worschech, and A. Forchel. Nonlinear photoluminescence spectra from a quantum-dot – cavity system: Interplay of pump-induced stimulated emission and anharmonic cavity QED. *Phys. Rev B*, **81**:033309, 2010.

Yoshie, T., A. Scherer, J. Heindrickson, G. Khitrova, H. M. Gibbs, G. Rupper, C. Ell, O. B. Shchekin, and D. G. Deppe. Vacuum Rabi splitting with a single quantum dot in a photonic crystal nanocavity. *Nature*, **432**:200, 2004.